Espresso Seminars

Theoretical Modelling of ECR Plasmas for Application to PANDORA

Bharat Mishra on behalf of the PANDORA Collaboration

Under The Supervision Of *David Mascali*

INFN – LNS, Catania, 5th April 2023

Talk Overview

Nuclear Astrophysics

R- and S-processes

Role of stellar β-decay rates and heavy element opacities

ECR Plasmas as Stellar Testbench

Physics and properties of ECR plasmas

Measurement of in-plasma decay rates using γ-tagging

Plasma diagnostics

Theoretical Modelling

Interplay between plasma environment and nuclear decay rates

Models as a tool to complement γ-tagging results

Extend theory to stellar interiors

Extract plasma parameters from diagnostics data

Advance fundamental research into ECRIS operation

Elements of Nuclear Astrophysics

S-process

Low neutron density (~ 10^5 – 10^6 cm^{-3}) and capture lifetime ~ 10^4 years

Absorption process competes with β and α-decay reactions – populates the valley of stability

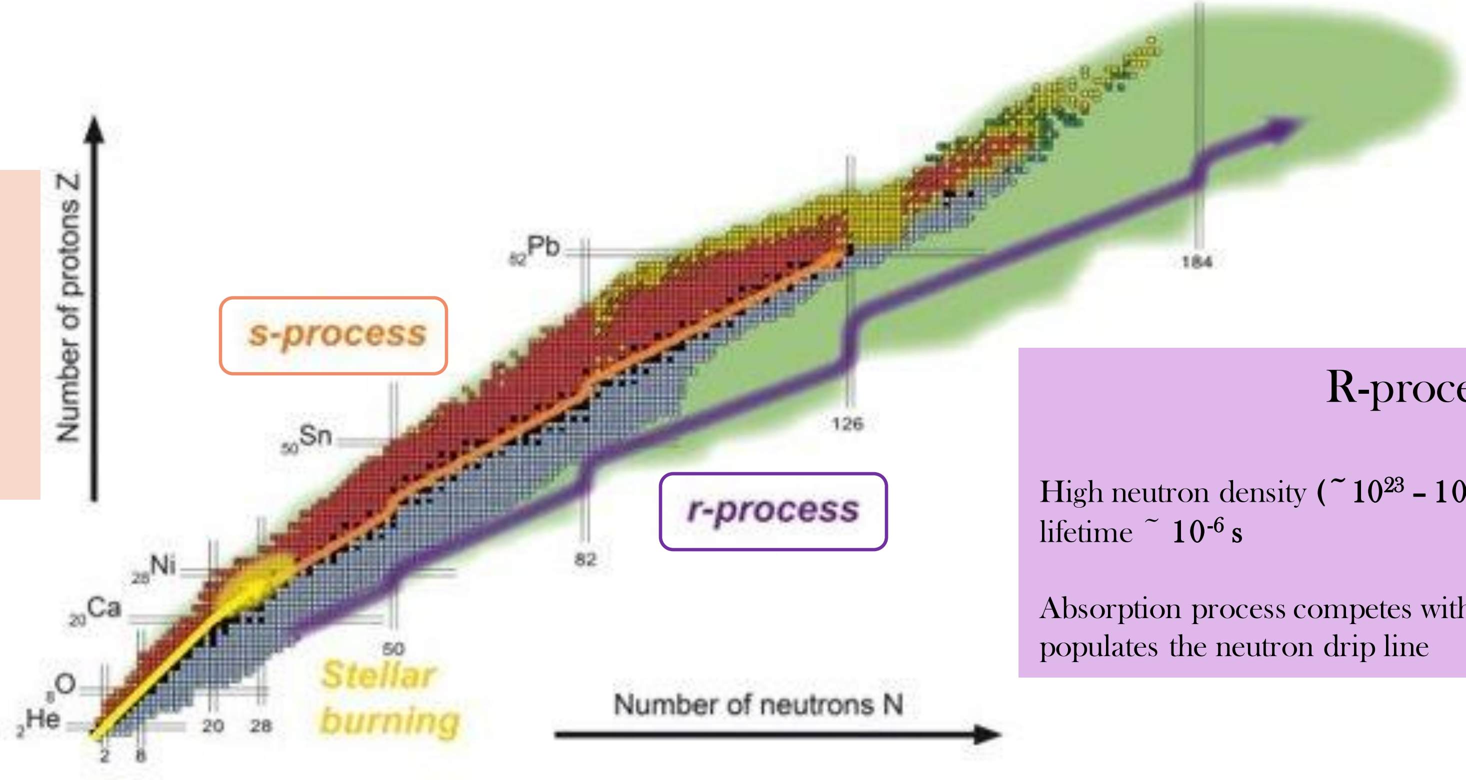

Nucleosynthesis chart showing neutron-capture processes [1]

R-process

High neutron density (~ 10^{23} – 10^{24} cm^{-3}) and capture lifetime ~ 10^{-6} s

Absorption process competes with inverse (γ,n) reaction – populates the neutron drip line

Elements of Nuclear Astrophysics

S-process

Production sites: AGB stars

β-decay $t_{1/2}$, MACS, neutron flux

R-process

Production sites: NS mergers and Kilonovae

KN light curves, heavy element opacity

Elemental abundance calculated using models requiring many inputs

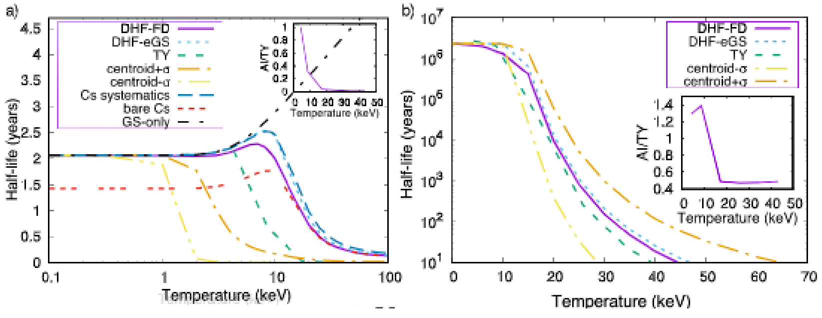

Variation of $t_{1/2}$ with plasma temperature [3]

The time-scale dynamics at which the KN peak occurs depends on the opacity

$$2.7\ \text{days} \left(\frac{\kappa}{1\ \text{cm}^2\ \text{g}^{-1}}\right)^{1/2} \left(\frac{M_{\text{ej}}}{0.01 M_\odot}\right)^{1/2} \left(\frac{v_{\text{ej}}}{0.1\,c}\right)^{-1/2}$$

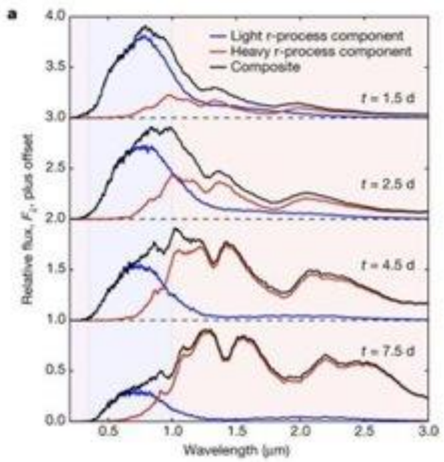

Variation of radiative flux with r-process nucleosynthesis elements [2]

Opacity and β-Decay Rates depend on plasma properties

Opacity content blatantly stolen from slides of Angelo Pidatella

[2] D. Kasen *et al.*, Nature 551, 80–84 (2017).
[3] S. Taioli *et al.*, ApJ 933, 158 (2022)

Electron Cyclotron Resonance Plasmas

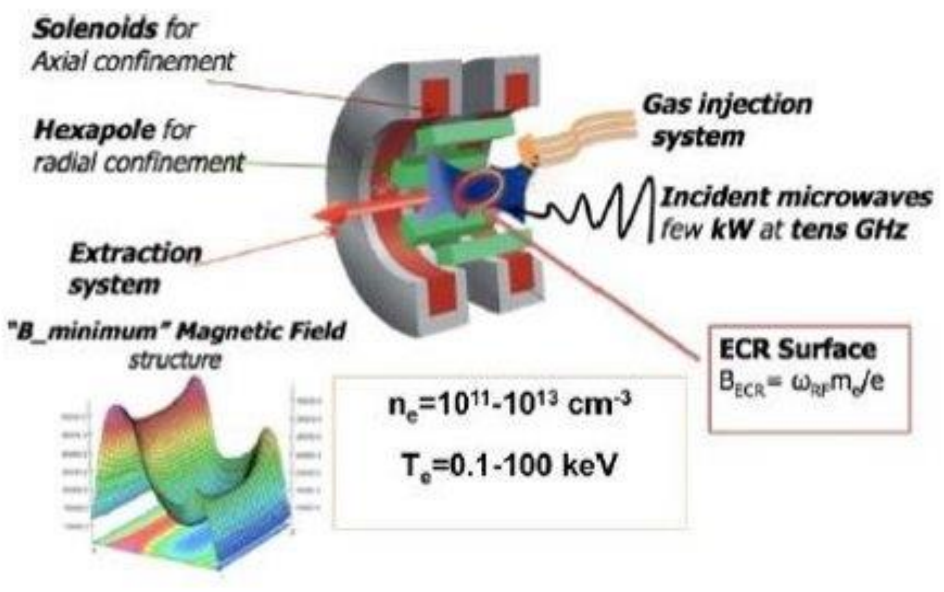

Schematic of ECRIS operation and global electron properties [4]

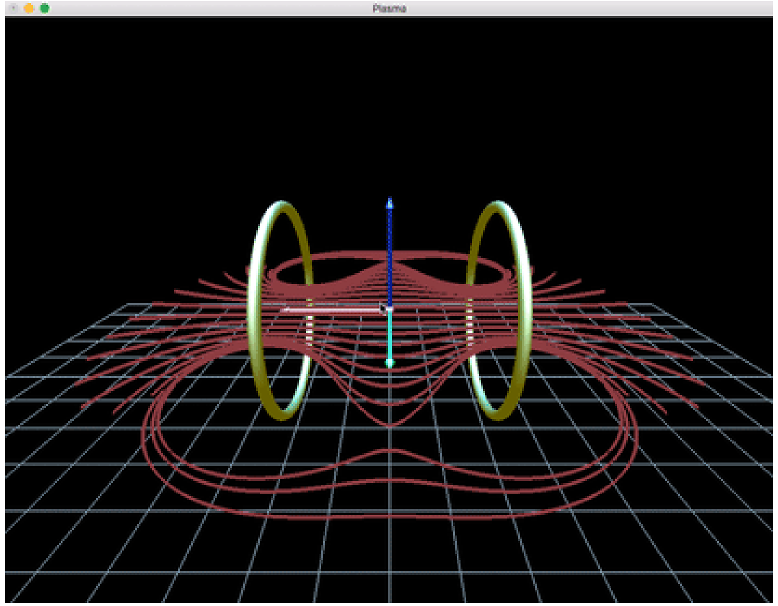

Electron trapping using B-min configuration

Longitudinal B-field → Electron gyration at $\omega_c = eB/m_e$ → Interaction with R-polarised microwave → Electron heating → PLASMA

B-min configuration → Adiabatic invariant → Electron trapping → PLASMA

[4] D. Mascali *et al.*, Eur. Phys. J. A 53, 145 (2017).

Properties of ECR Plasmas

Electrons are heated to high energies ($k_B T_e$ between 0.1 - 100 keV)

Electron density n_e reaches 10^{11} – 10^{13} cm^{-3}

Ions are cold and stationary relative to electrons

Stellar densities are much higher (n_e, n_i ~ 10^{20} – 10^{22} cm^{-3})

Both electrons and ions are energetic

ECR plasmas can emulate stellar interiors to some degree

Energetic electrons (~ keV) and radiation interact with ions in NLTE to produce CSD and LPD

Ions and electrons interact with each other and radiation to produce LTE CSD and LPD

PANDORA

Plasmas for **A**strophysics, **N**uclear **D**ecay **O**bservations and **R**adiation for **A**rchaeometry

n_e: 10^{12} – 10^{14} cm^{-3}
T_e: 0.01 – 100 keV

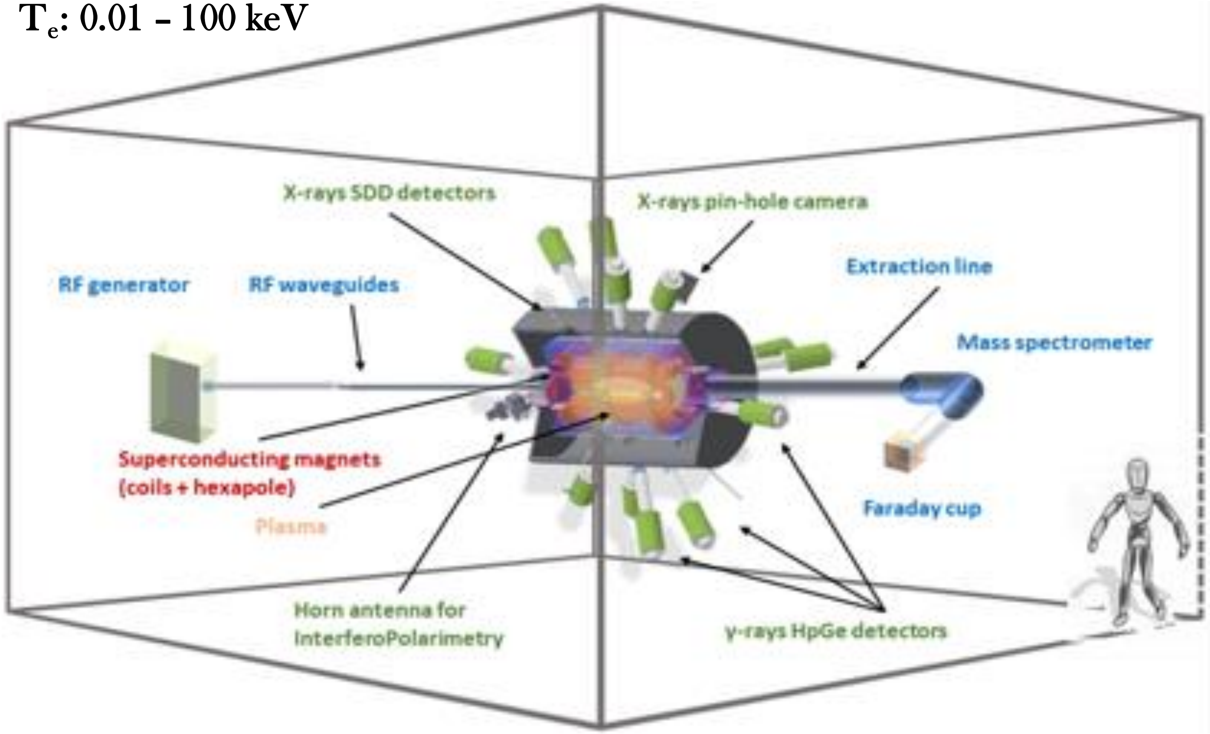

Two grand classes of in-plasma phenomena to be studied:

- β-decay rates of radioisotopes in stellar atmospheres for s-process branching
- opacity of heavy elements in early-stage KN for r-process nucleosynthesis

γ -Tagging and $T_{1/2}$ Measurement

ECR magnetoplasma can be maintained in MHD equilibrium for days or even weeks

$$\frac{dN}{dt} = \lambda n_i V \quad \Rightarrow \quad N(T_{meas}) = \lambda n_i V_{plasma} T_{meas}$$

$\lambda n_i V$ is constant

- *Isotope activity* $\lambda \equiv \lambda(T, n)$
- *Density of the isotope in the plasma (const.)*
- *Plasma volume (const.)*

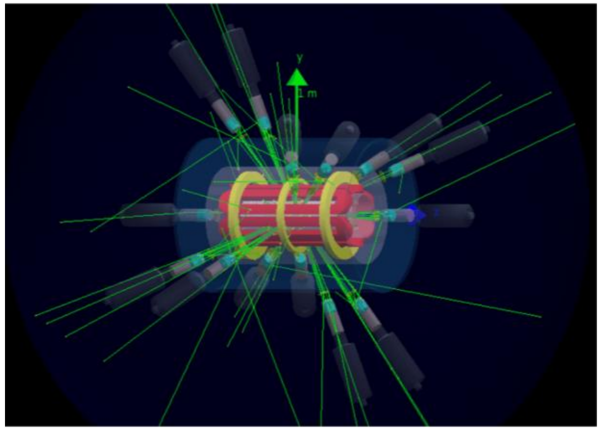

Numerical simulations to determine detection efficiency according to chosen plasma model - 14 HpGe detectors [5]

1% Lu of 10^{13} cm^{-3} (V_p = 1500 cm^3)

E_γ = 202.88 and 306.78 keV

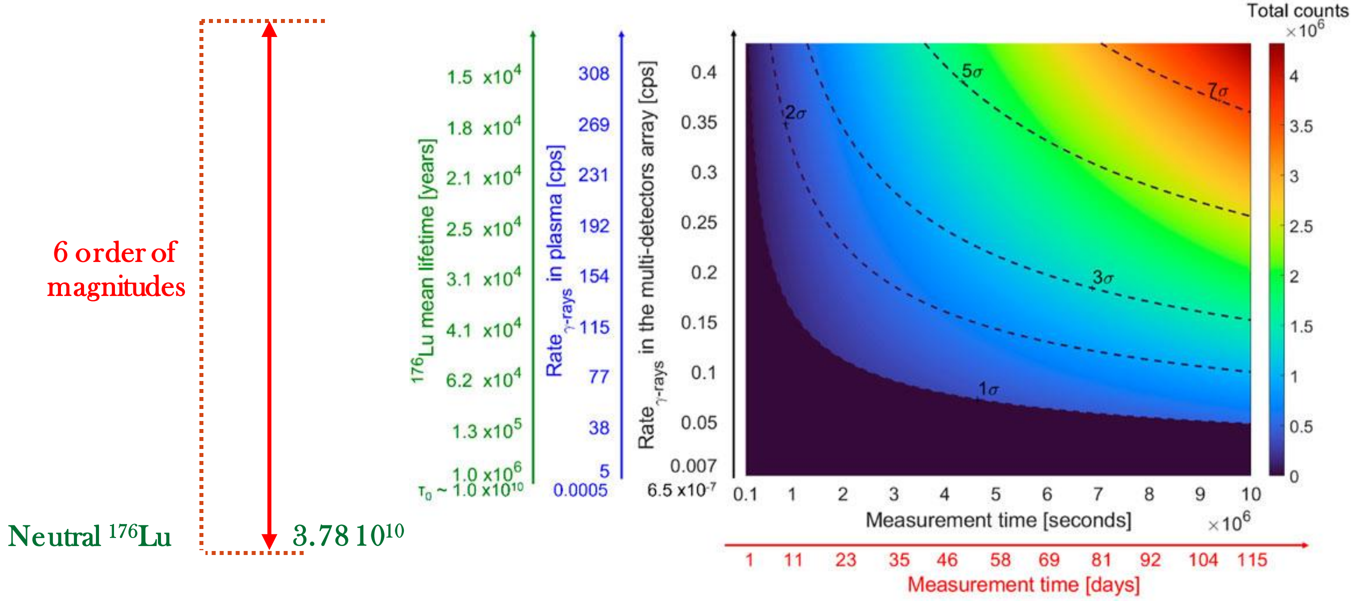

Iso-significance contour plots for ^{176}Lu isotope showing measurement time required to overcome background, as a function of lifetime and significance level [6]

[5] D. Mascali *et al*, Universe 8, 80, 2022
[6] E. Naselli, Frontiers In Phys., special issue (2022)

Plasma Diagnostics

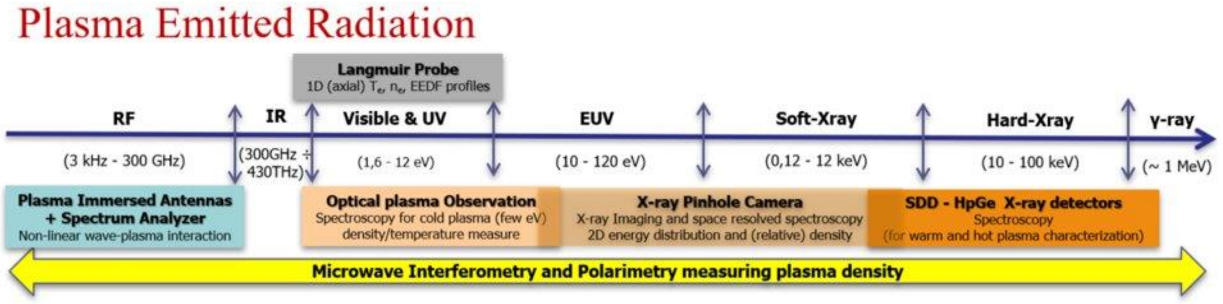

Diagnostic tool	Sensitive Range	Measurement	Resolution & Meas. Error
SDD	1.0 ÷ 30 keV	Volumetric soft X-ray Spectroscopy: warm electrons temperature and density	Res. ~ 120 eV $\epsilon_{n_e} \sim 7\%$, $\epsilon_{T_e} \sim 5\%$
HpGe	30 ÷ 400 keV	Volumetric hard X-ray Spectroscopy: hard electrons temperature and density	Res. ~ 200 eV $\epsilon_{n_e} \sim 7\%$, $\epsilon_{T_e} \sim 5\%$
Visible Light Camera	1.0 ÷ 12 eV	Optical Emission Spectroscopy: cold electrons temperature and density	$\Delta\lambda = 0.04$nm R=12500
Microwave Interferometer	K-band 18 ÷ 26.5 GHz	Interferometric measurement: line integrated total density	$\epsilon_{n_e} \sim 50\%$
Microwave Polarimeter	K-band 18 ÷ 26.5 GHz	Faraday-rotation measurement: line integrated total density	$\epsilon_{n_e} \sim 25\%$
X-ray pin-hole camera	2 ÷ 15 keV	2D Space-resolved spectroscopy soft X-ray Imaging and plasma structure	Energy Res. ~ 0.326 keV Spatial Res. ~ 0.56 mm
Multi-pins RF probe + Spectrum Analyzer (SA)	10 ÷ 26.5 GHz *(probe)*	Frequency-resolved Spectroscopy plasma emitted EM wave in GHz range	SA Resolution bandwidth: RBW = 3 MHz
Multi-pins RF probe + Scope + HpGe	10 ÷ 26.5 GHz *(probe)*	Time-resolved X-ray Spectroscopy	80 Gs/s *(scope)* time scales below ns

Plasma Diagnostics – Warm Electrons

High energy bremsstrahlung and contribution from extraction plate

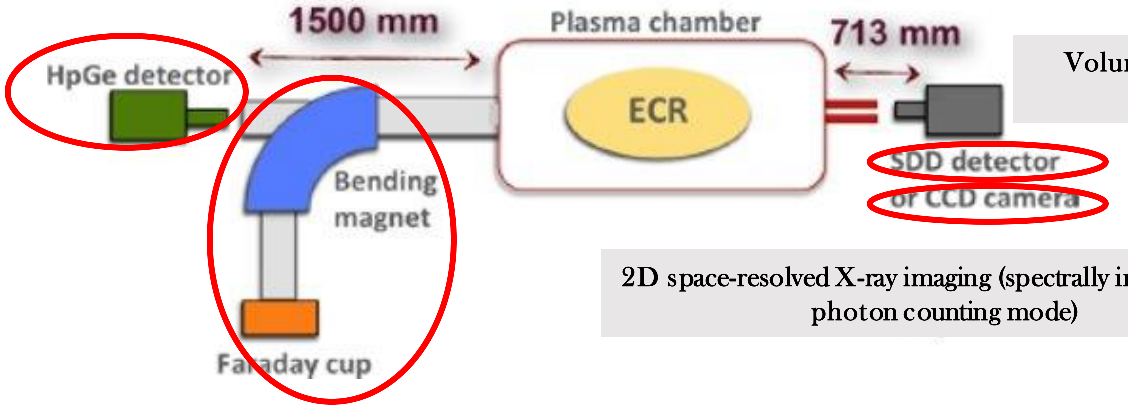

Volumetric fluorescence and low energy bremsstrahlung emission

2D space-resolved X-ray imaging (spectrally integrated and photon counting mode)

Measuring ion currents (total and individual charge states)

Schematic of X-ray experimental setup showing various detectors used and distances [7]

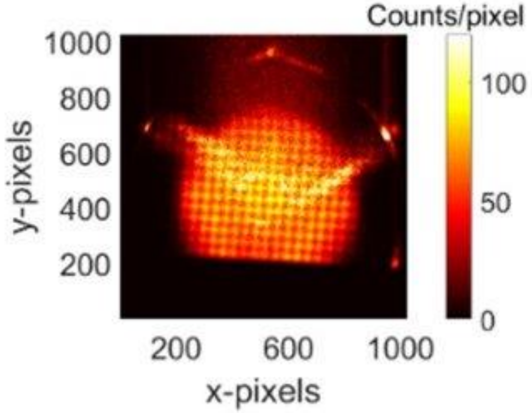

2D X-ray imaging (top) and soft X-ray spectrum (below) [8]

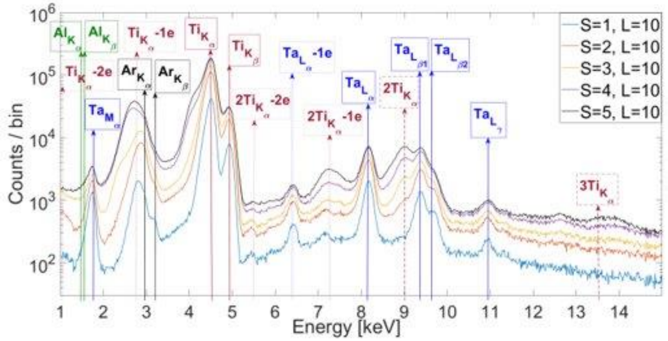

[7] D. Mascali et al, Rev. Sci. Instrum. 87, 02A510 (2016).
[8] E. Naselli et al, Condens. Matter 1, 0 (2021).

ECR Plasma Modelling – Why?

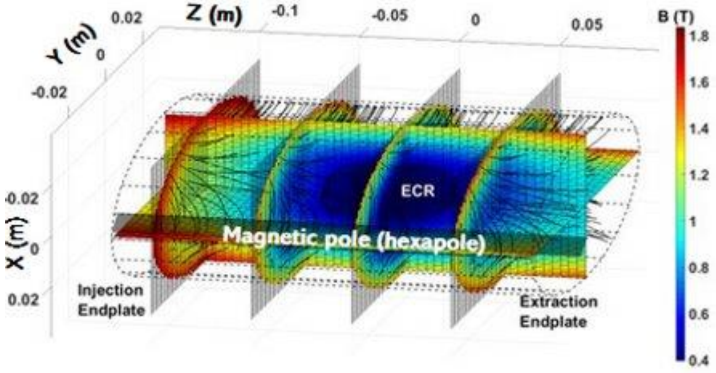

B-field surfaces in a plasma chamber with the closed ECR surface [9]

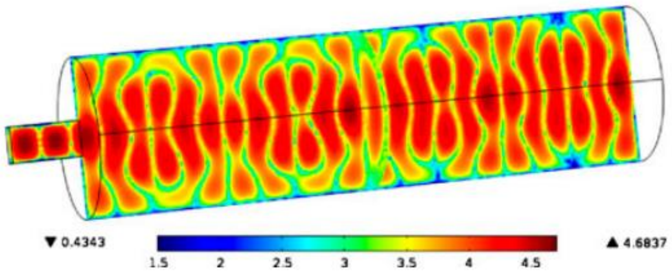

Mode-like EM field structure in plasma chamber under vacuum [10]

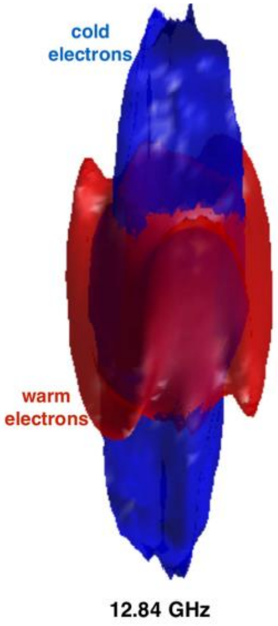

3D structure of electrons from simulations – the spatial anisotropy and non-homogeneity with respect to density and energy are visible [11]

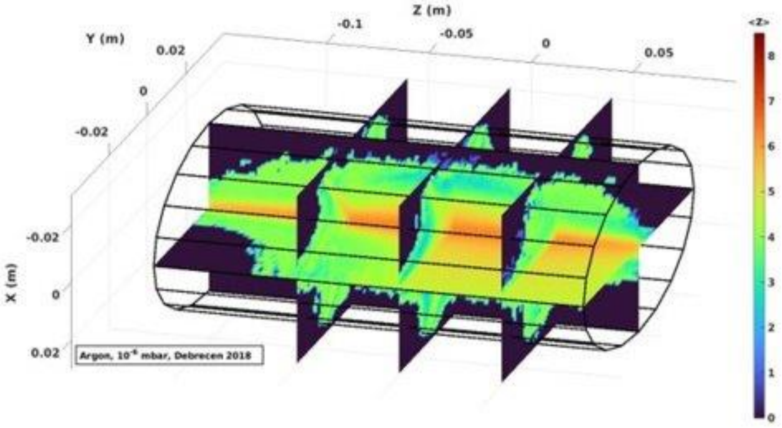

3D structure of ions from simulations – the anisotropy is a direct consequence of non-homogenous electron distribution and complex particle transport [12]

[9] B. Mishra *et al*, Frontiers in Phys., special issue (2022)
[10] G. Torrisi *et al*, JEWA 28, 9 (2014)
[11] R. Racz *et al*, Plasma Sources Sci. Technol. 26, 075011 (2017)
[12] B. Mishra, EPJ Web of Conferences, 2022.

ECR Plasma Modelling – Why?

ECR plasmas properties are non-uniform. Models can:

(1) Help calculate space-resolved decay rates and opacities

(2) Connect laboratory and stellar plasma theory

(3) Complement γ-tagging results

(4) Couple with diagnostics for extracting plasma parameters

(5) Improve fundamental understanding of ECRIS devices

In-Plasma β-Decay Rates

NEUTRAL ATOM		ION
${}^{A}_{Z}X_N \rightarrow {}^{A}_{Z+1}Y_{N-1} + e^-_f + \bar{\nu}_e$	**c. d.**	$({}^{A}_{Z}X_N)^{i,j} \rightarrow ({}^{A}_{Z+1}Y_{N-1})^{i+1,j'} + e^-_f + \bar{\nu}_e$
${}^{A}_{Z}X_N \rightarrow {}^{A}_{Z+1}Y_{N-1} + e^-_b + \bar{\nu}_e$	**b. d.**	$({}^{A}_{Z}X_N)^{i,j} \rightarrow ({}^{A}_{Z+1}Y_{N-1})^{i,j'} + e^-_b + \bar{\nu}_e$
${}^{A}_{Z}X_N + e^-_b \rightarrow {}^{A}_{Z-1}Y_{N+1} + \nu_e$	**b. c.**	$({}^{A}_{Z}X_N)^{i,j} + e^-_f \rightarrow ({}^{A}_{Z-1}Y_{N+1})^{i,j'} + \nu_e$
${}^{A}_{Z}X_N + e^-_f \rightarrow {}^{A}_{Z-1}Y_{N+1} + \nu_e$	**c. c.**	$({}^{A}_{Z}X_N)^{i,j} + e^-_b \rightarrow ({}^{A}_{Z-1}Y_{N+1})^{i-1,j'} + \nu_e$

$$Q_0 = \begin{cases} m_0({}^{A}_{Z}X_N)c^2 - m_0({}^{A}_{Z+1/Z-1}Y_{N-1/N+1})c^2 \\ m_0({}^{A}_{Z}X_N)c^2 - m_0({}^{A}_{Z+1/Z-1}Y_{N-1/N+1})c^2 + K_{e_f} \end{cases}$$

Mass of neutral atom at ground state

Kinetic energy of continuum electron

$$Q = Q_0 + (E^*_{X,K} - E^*_{Y,K'}) + (\epsilon^{i,j} - \epsilon^{i',j'}) + (\Delta_X - \Delta_Y)$$

Nuclear level energy

Ion level energy

IPD contribution

In-Plasma β-Decay Rates

NEUTRAL ATOM

$$f_{if(m)}t_{1/2} = \frac{(\ln 2)2\pi^3\hbar^7}{g^2 m_e^5 c^4 |M_{if}^{L(m)}|^2}$$

Type of transition (allowed, unique first forbidden...) - Determines shape factor $S_m(x)$

Nuclear Matrix Element (NME)

ION

Continuum decay

$$f^*_{IF(m)} = \sum_{ij} p_{ij} \int_1^{W_{max}(ij)} (W^2-1)^{1/2} W (W_{max}(ij)-W)^2 F_0 S_{(m)}(ij) f_d(ij) \mathrm{d}W$$

Continuum capture

$$f^*_{IF(m)} = \sum_{ij} p_{ij} \int_{W_{min}(ij)}^{\infty} (W^2-1)^{1/2} W (Q(ij)/m_e c^2)^2 F_0 S_{(m)}(ij) f_c(ij) \mathrm{d}W$$

Bound decay/ Bound capture

$$f^*_{IF(m)} = \sum_{ij} p_{ij} \sum_{x(ij)} \sigma_x \frac{\pi}{2} [g_x \, or \, f_x]^2 (Q(ij)/m_e c^2)^2 S_{(m)x(ij)}$$

PLASMA

SUMMATION OVER ALL POSSIBLE DECAY CHANNELS

$$\lambda_{tot} = \sum \frac{\ln 2}{f_{IF(m)} t_{1/2}} f^*_{IF(m)}$$

[16] K. Takahashi and K. Yokoi, Nucl. Phys. A404 (1983), 578.
[17] J. Bahcall, Phys. Rev. 128 (1962), 3.

In-Plasma β-Decay Rates

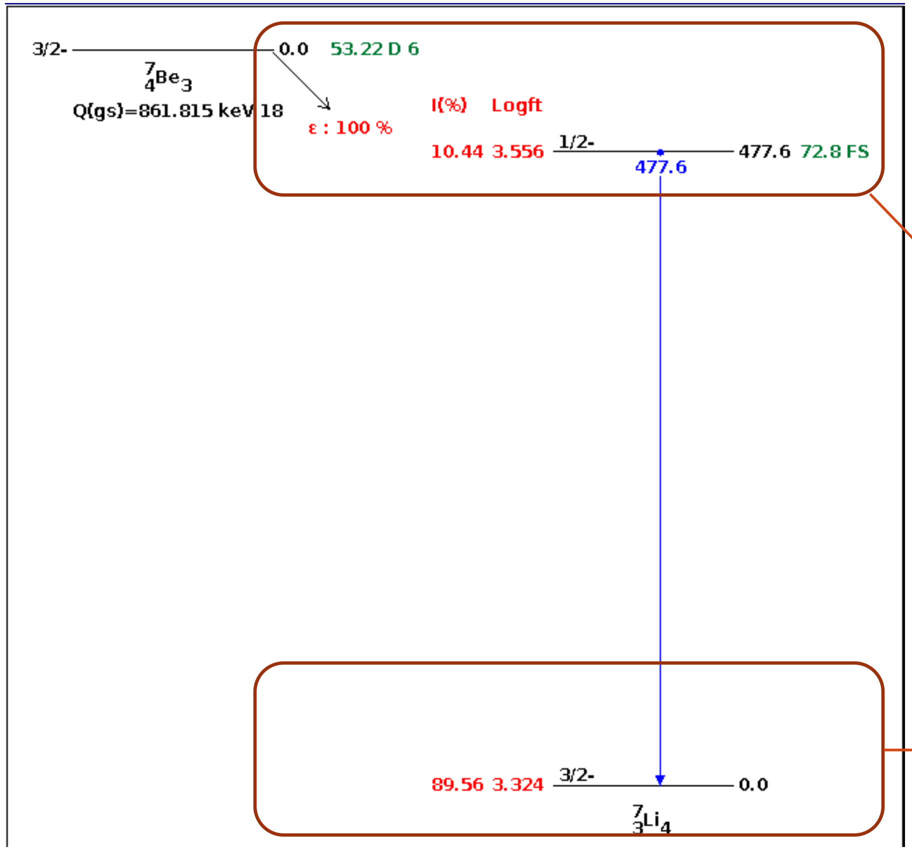

^{7}Be decay scheme [18]

^{7}Be undergoes electron capture to ^{7}Li

Contribution from both continuum and bound state electron capture

Information needed: log ft values

Correlated with the strength of the decay and the nuclear matrix element

$3/2^-$ -> $1/2^-$ (gs -> es transition)
Allowed transition
Log ft = 3.556

$3/2^-$ -> $3/2^-$ (gs -> gs transition)
Allowed transition
Log ft = 3.324

NO OTHER DECAY CHANNEL CONSIDERED

[18] NNDC Nuclear Data Chart

In-Plasma β-Decay Rates

The lepton phase volume quantifies the number of ways a decay can occur. The phase volume changes with variations in atomic configuration, depending on type of decay

Information needed: level probability distribution (LPD), orbital occupancy, orbital electron wavefunction, decay energy and shape factor

$$f^*_{IF(m)} = \sum_{ij} p_{ij} \sum_{x(ij)} \sigma_x \frac{\pi}{2} [g_x \; or \; f_x]^2 (Q(ij)/m_e c^2)^2 S_{(m)x(ij)}$$

(b) Shape factor describing compatibility between nuclear and lepton wavefunction

(e) Probability distribution of various charge states and levels of isotope

(d) Occupancy of orbital contributing to certain decay within relevant ionic configuration

(c) Larger of squared radial component of electron wavefunction evaluated on nuclear surface

(a) Q-value of decay when isotope in (i,j) charge state and level configuration

[16] K. Takahashi and K. Yokoi, Nucl. Phys. A404 (1983), 578.

In-Plasma β-Decay Rates

$$Q = Q_0 + (E^*_{X,K} - E^*_{Y,K'}) + (\epsilon^{i,j} - \epsilon^{i',j'}) + (\Delta_X - \Delta_Y)$$

The decay energy depends on not just the difference in nuclear masses, but on the overall system energy which includes atomic/ionic energy

Information needed: energy of different atomic configurations of parent system and coupling with daughter system

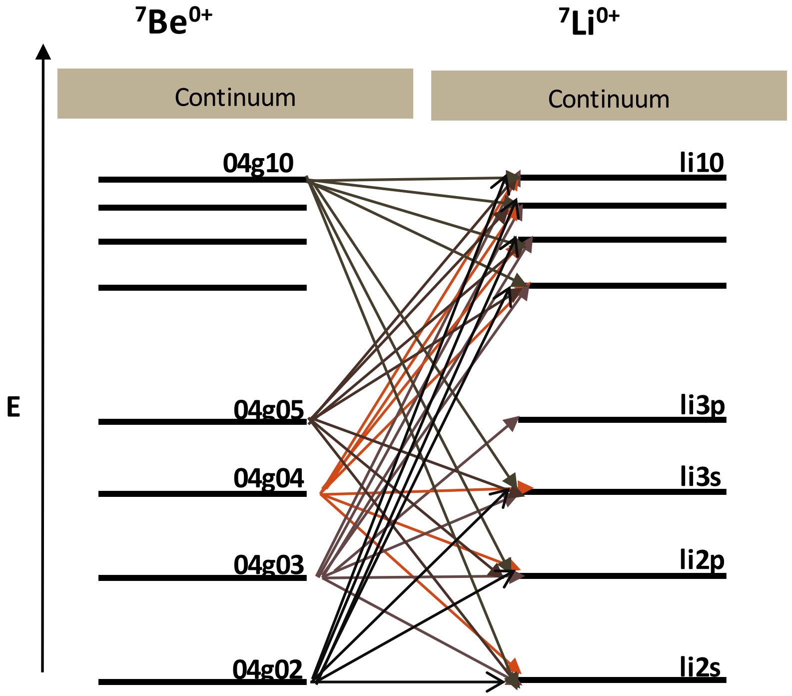

^7Be - ^7Li level coupling schematic for K- and L-shell capture (neutral ion)

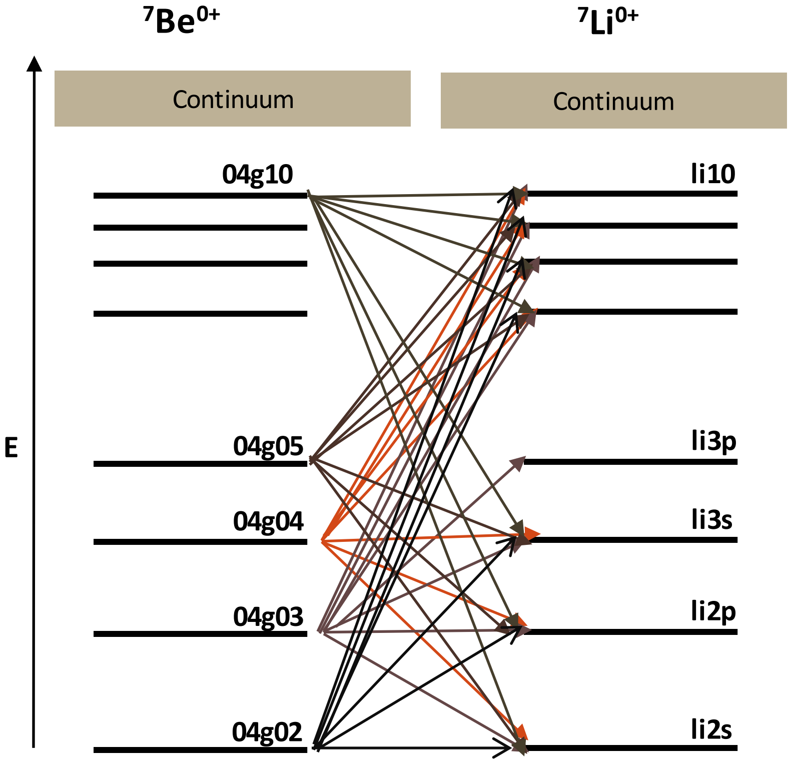

All configurations should have at least one K-shell electron

No selection on daughter configuration
K-shell vacant states autoionising

K-SHELL CAPTURE

All configurations should have at least one L-shell electron

No selection on daughter configuration
L-shell vacant states autoionising

In-Plasma β-Decay Rates

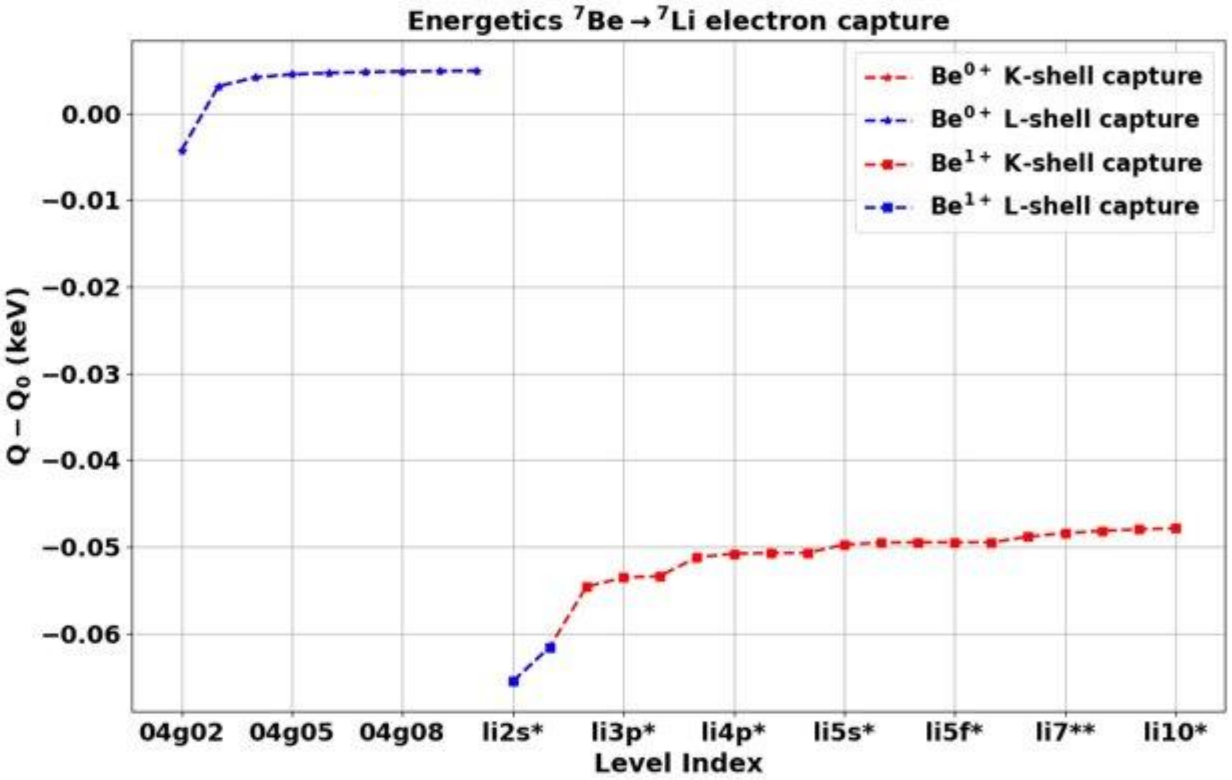

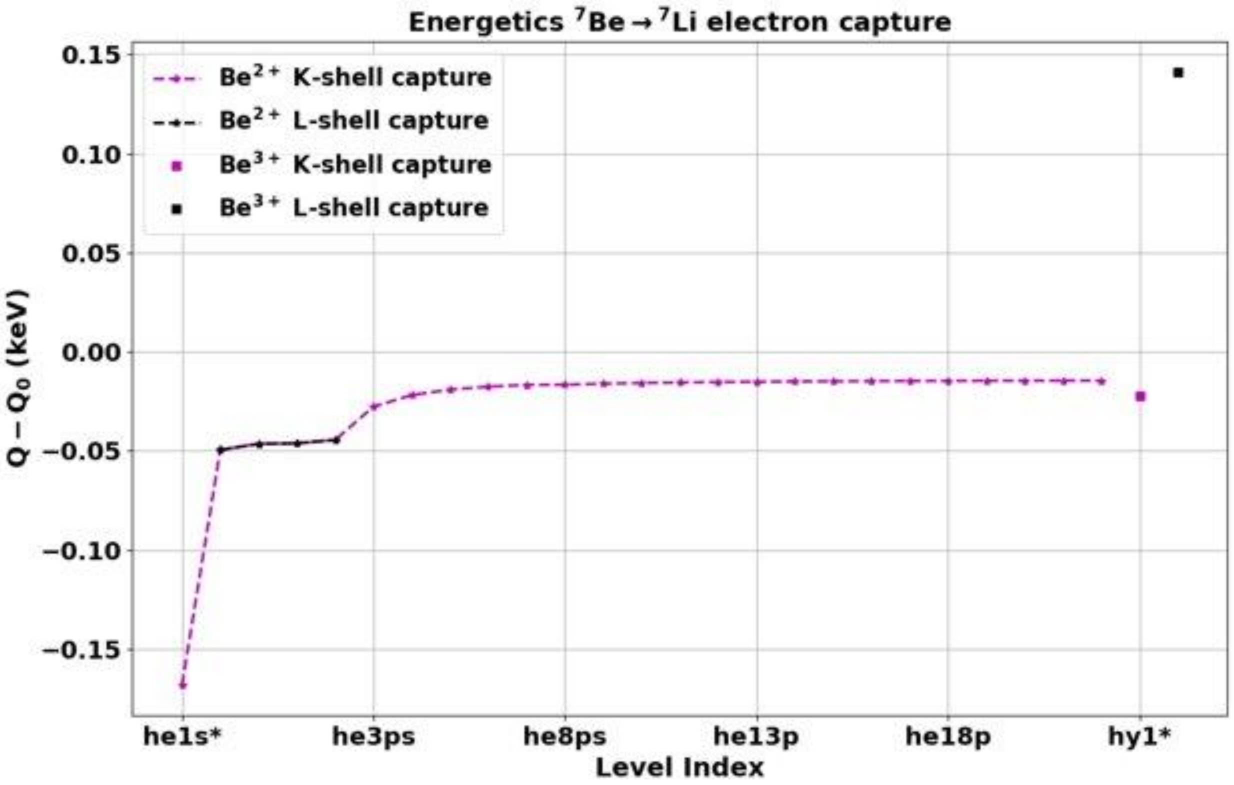

^{7}Be decay Q-value as a function of charge state and level for neutral and 1+ (left) and 2+ and 3+ (right)

In-Plasma β-Decay Rates

Conservation of total angular momentum implies that only certain electron orbitals can interact with the nucleus, depending on the spin and parity of the decay

Information needed: spin-parity of electron orbitals and decay transition

$$S_{(m)x} = \begin{cases} 1 & \text{for } m = a, nu \text{ and } x = ns_{1/2}, np_{1/2} \\ q^2 & \text{for } m = u \text{ and } x = ns_{1/2}, np_{1/2} \\ 9/R^2 & \text{for } m = u \text{ and } x = np_{3/2}, nd_{3/2} \\ 0 & \text{otherwise.} \end{cases}$$

[16] K. Takashi and K. Yokoi, Nuclear Physics A404 (1983) 578

In-Plasma β-Decay Rates

The probability of electron capture from bound states depends on the square of the radial component of the orbital wavefunction evaluated on the nuclear surface

Information needed: formalism for radial wavefunctions of different orbitals

Radial component of Dirac equation – Coupled differential equations

$$\frac{\mathrm{d}P(r)}{\mathrm{d}r} = -\frac{\kappa}{r}P(r) - \left(2c + \frac{V-\epsilon}{c}\right)Q(r) \qquad \frac{\mathrm{d}Q(r)}{\mathrm{d}r} = \frac{\kappa}{r}Q(r) + \left(\frac{V-\epsilon}{c}\right)P(r)$$

For V = Z/r (in atomic units)

$$P(r) = \left(1 - \frac{\epsilon}{c^2}\right)^{1/2} \xi \left(\frac{\rho}{N}\right)^{\gamma} \mathrm{e}^{-\rho/2N}[-n_r F_1 + (N-\kappa)F_2]$$

$$Q(r) = \left(\frac{\epsilon}{c^2}\right)^{1/2} \xi \left(\frac{\rho}{N}\right)^{\gamma} \mathrm{e}^{-\rho/2N}[n_r F_1 + (N-\kappa)F_2]$$

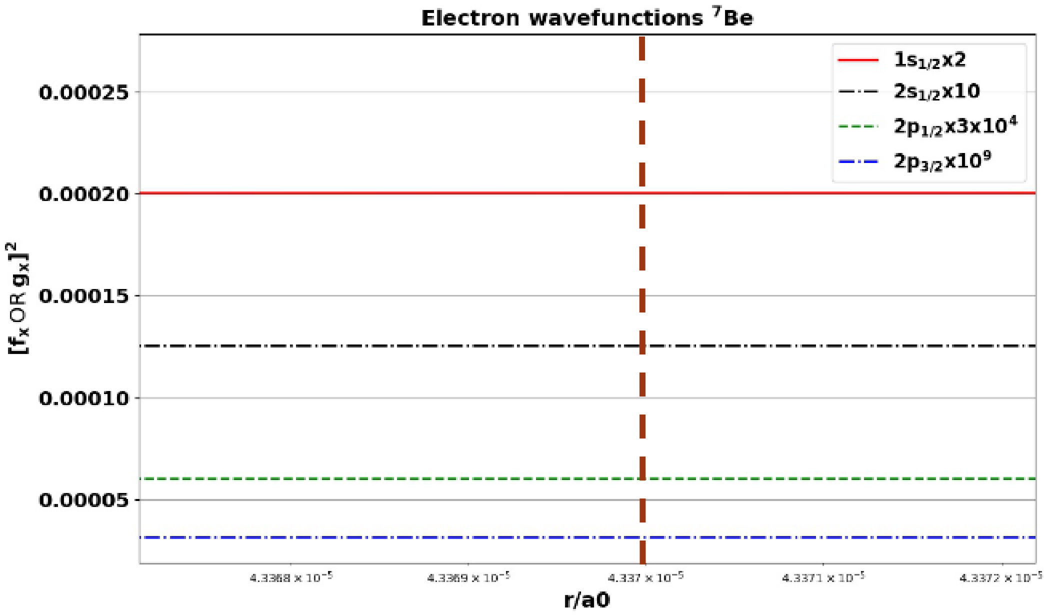

Larger of f_x^2 or g_x^2 as calculated for ^{7}Be taking $R = R_0A^{1/3}$

[18] V. M. Burke and I. P. Grant, Proceedings of the Physical Society 90 (1967) 297

In-Plasma β-Decay Rates

The probability of electron capture from bound states also depends on the occupancy of the relevant orbital

Information needed: Occupancy of relevant orbitals as a function of the level configuration and ion charge state

li2s level in $^7Be^{1+}$ - 2e$^-$ in *1s*, 1e$^-$ in *2s*
$1s_{1/2}$ occupancy = 1
$2s_{1/2}$ occupancy = 0.5
$2p_{1/2}$ occupancy = $2p_{3/2}$ occupancy = 0

Suppressed L-capture

li2p level in $^7Be^{1+}$ - 2e$^-$ in *1s*, 1e$^-$ in *2p*
$1s_{1/2}$ occupancy = 1
$2s_{1/2}$ occupancy = 0
$2p_{1/2}$ occupancy = $2p_{3/2}$ occupancy = 0.167

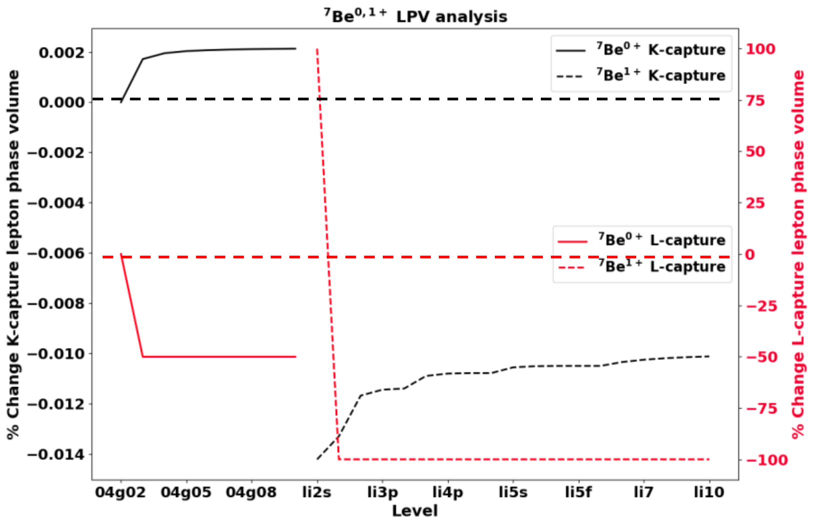

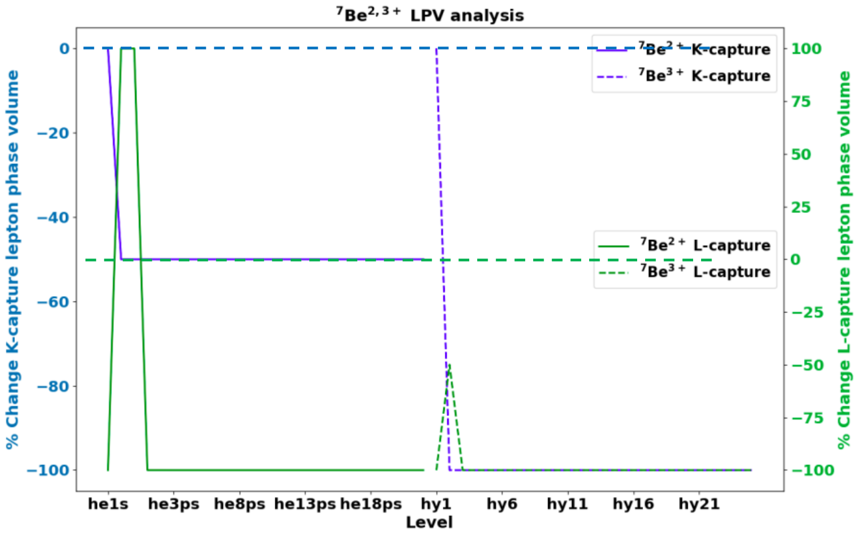

% change in lepton phase volume can be quite pronounced for some configurations which are accessible by plasma

Levels can be combined into super-groups based on similarity in lepton phase volume – computational advantage

In-Plasma β-Decay Rates

The ion CSD and LPD strongly depends on electron density and temperature

Information needed: CSD and LPD of ^{7}Be for various n_e and T_e (calculated using FLYCHK)

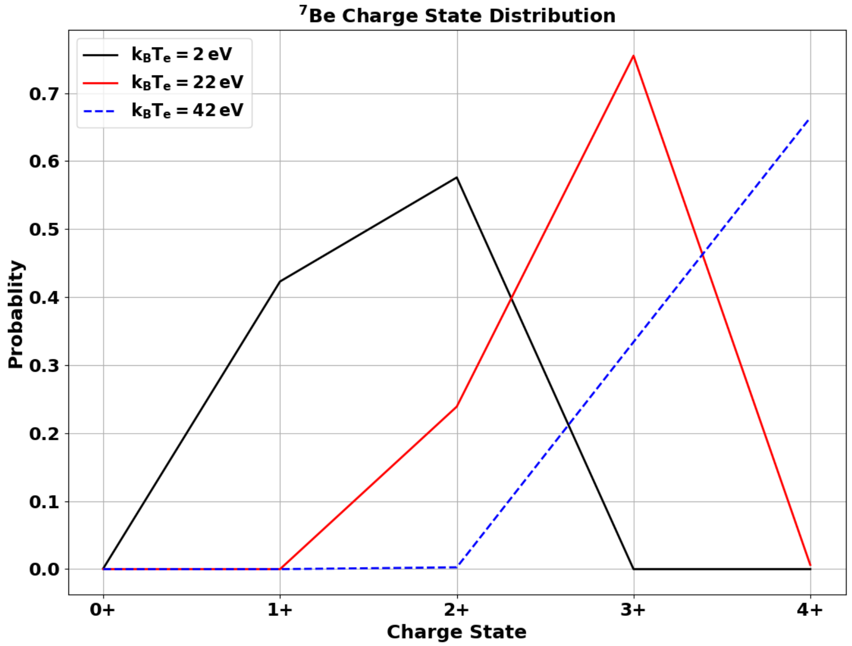

CSD of ^{7}Be for different temperatures as calculated by FLYCHK (no effect of density)

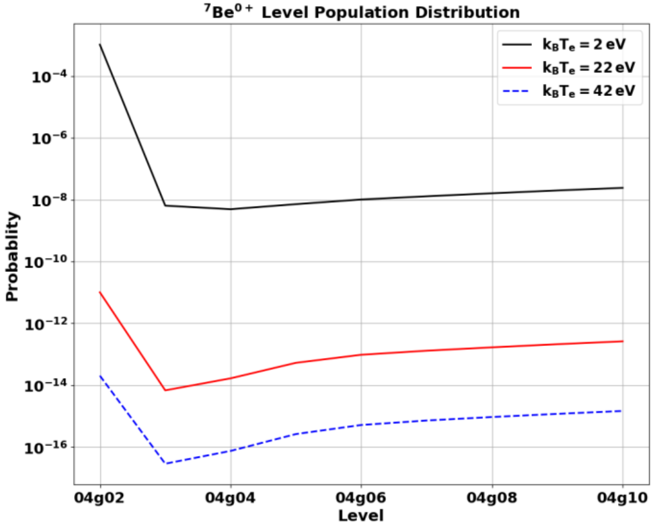

LPD of $^{7}Be^{0+}$ and $^{7}Be^{3+}$ for different temperatures as calculated by FLYCHK (no effect of density)

CSD and LPD calculated using grid of density and temperature values in FLYCHK under LTE approximation

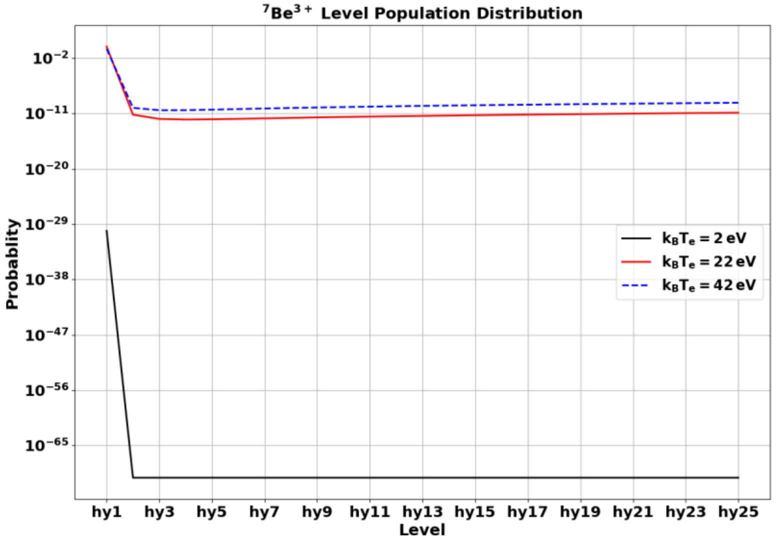

In-Plasma β-Decay Rates

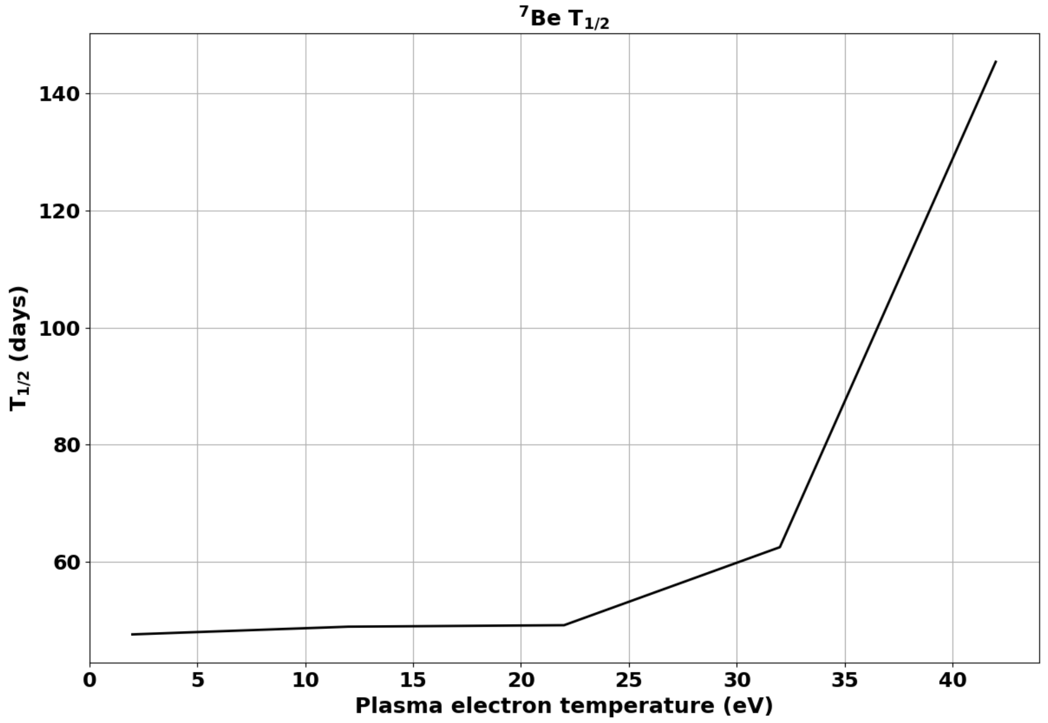

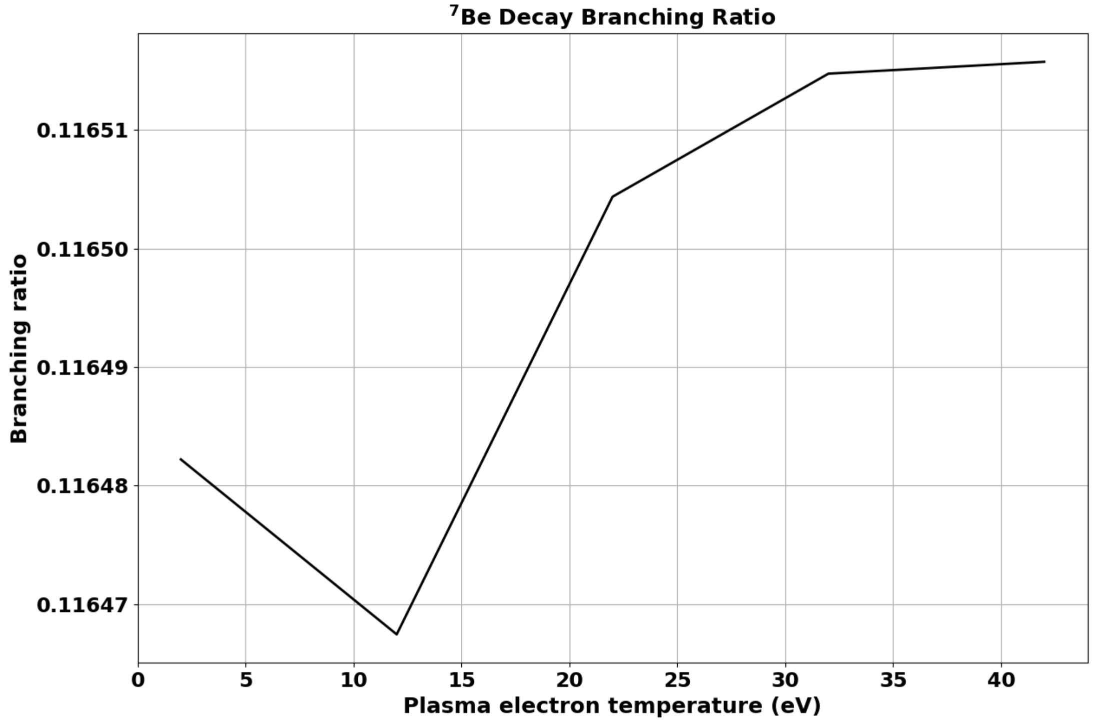

^{7}Be ground state (neutral and 04g02 level config)

$T_{1/2}$ calculated = 47.4 days
Branching ratio = 11.6 %

$T_{1/2}$ measured [7] = 53 ± 6 days
Branching ratio = 10.7 ± 0.2%

[19] G.J. Matthews, R.C. Haight, R.G. Lanier and R.M White, Physical Review C 28 (1983) 2

In-Plasma β-Decay Rates

$$f^*_{IF(m)} = \sum_{ij} p_{ij} \int_1^{W_{max}(ij)} (W^2-1)^{1/2} W (W_{max}(ij)-W)^2 F_0 S_{(m)}(ij) f_d(ij) \mathrm{d}W$$

$$f^*_{IF(m)} = \sum_{ij} p_{ij} \int_{W_{min}(ij)}^{\infty} (W^2-1)^{1/2} W (Q(ij)/m_e c^2)^2 F_0 S_{(m)}(ij) f_c(ij) \mathrm{d}W$$

$$f^*_{IF(m)} = \sum_{ij} p_{ij} \sum_{x(ij)} \sigma_x \frac{\pi}{2} [g_x \, or \, f_x]^2 (Q(ij)/m_e c^2)^2 S_{(m)x(ij)}$$

CALCULATING THESE IN ECR PLASMA IS THE ULTIMATE GOAL!

[16] K. Takahashi and K. Yokoi, Nucl. Phys. A404 (1983), 578.

Self-Consistent Steady-State Electron Simulations

Schematic of COMSOL Multiphysics© + MATLAB©
self-consistent numerical modelling for electrons

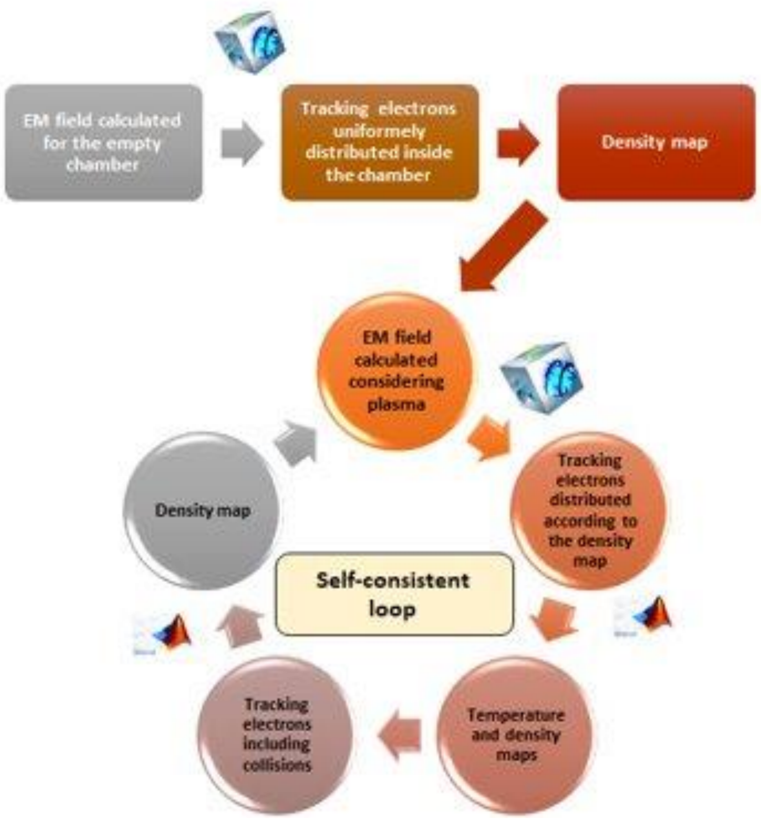

Vlasov equation

$$\frac{\partial f_\alpha}{\partial t} + \boldsymbol{v} \cdot \frac{\partial f_\alpha}{\partial \boldsymbol{r}} + \frac{q_\alpha}{m_\alpha}(\boldsymbol{E} + \boldsymbol{v} \times \boldsymbol{B}) \cdot \frac{\partial f_\alpha}{\partial \boldsymbol{v}} = 0$$

+

Fokker-Planck collisions

$$\frac{1}{\Gamma}\mathbb{C} = -\frac{\partial}{\partial \mathbf{v}} \cdot \left(f \frac{\partial \mathscr{H}}{\partial \mathbf{v}}\right) + \frac{1}{2}\frac{\partial^2}{\partial \mathbf{v} \partial \mathbf{v}} : \left(f \frac{\partial^2 \mathscr{G}}{\partial \mathbf{v} \partial \mathbf{v}}\right)$$

+

Maxwell equations

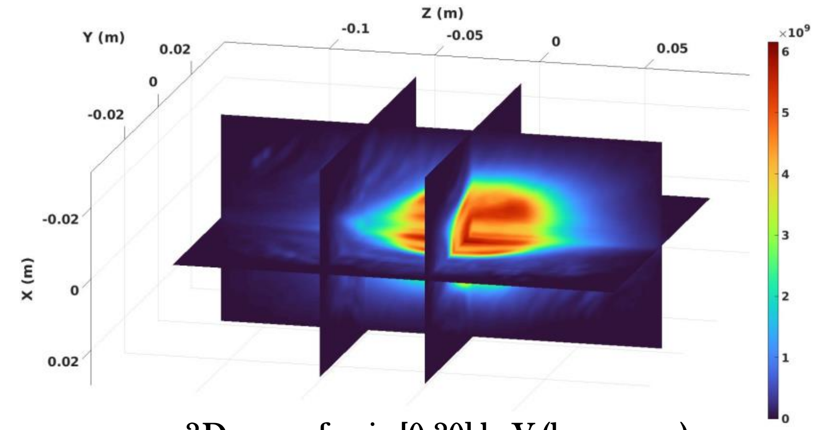

3D map of n_e in [0,30] keV (low power)

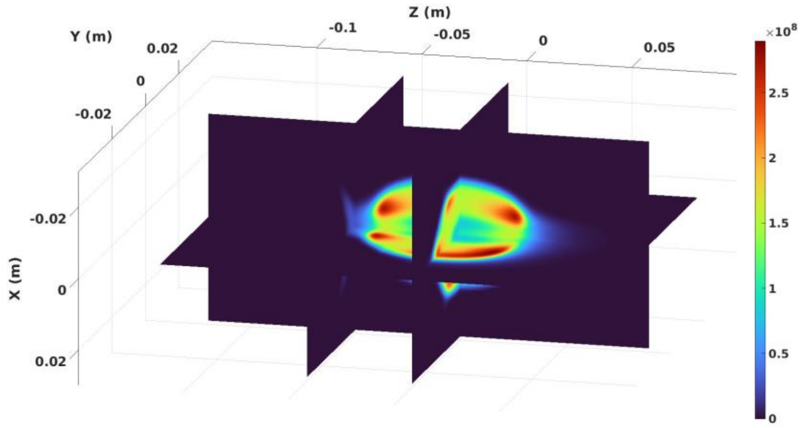

3D map of n_e in [1,100] keV (high power)

[13] D. Mascali *et al*, EPJ D, 69:27 (2015)
[14] A. Galatà *et al*, Plasma Sources Sci. Tech. 25, 045007 (2016)

Self-Consistent Electron-Ion Simulations

BUFFER IONS BALANCE EQUATION:

$$\frac{\mathrm{d}n_i}{\mathrm{d}t} = n_{i-1}n_e\gamma_{i-1,i} - n_i n_e \gamma_{i,i+1} + n_{i+1}n_0 E_{i+1,i} - n_i n_0 E_{i,i-1} - \frac{n_i}{\tau_i}$$

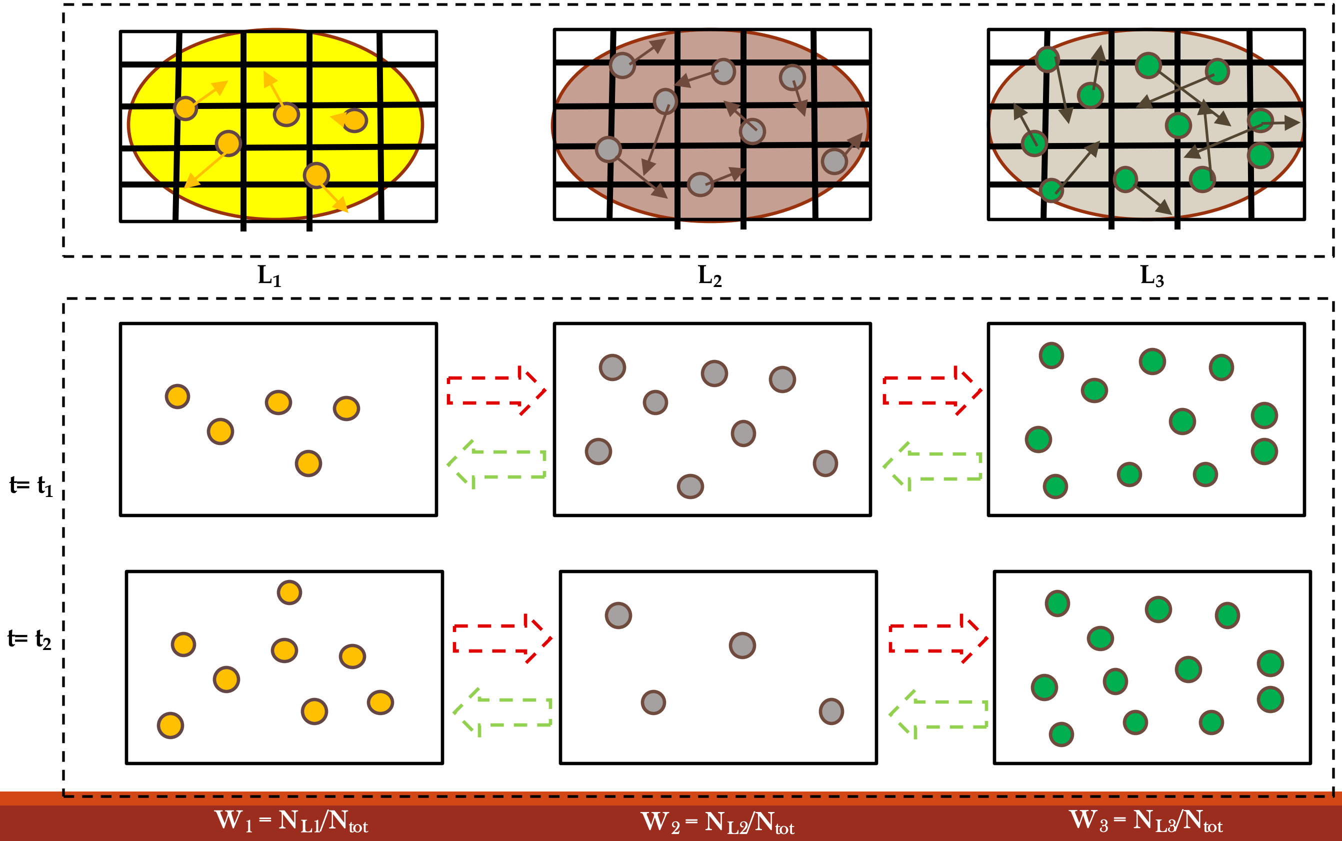

Particle transport under EM fields with collision to generate 3D spatial distribution (occupation maps)

Constant monitoring of loss/gain of macroparticles between various levels to calculate relative weight of each level

Forward reactions – ionisation, excitation, absorption
Backward reactions – charge exchange, de-excitation, spontaneous emission

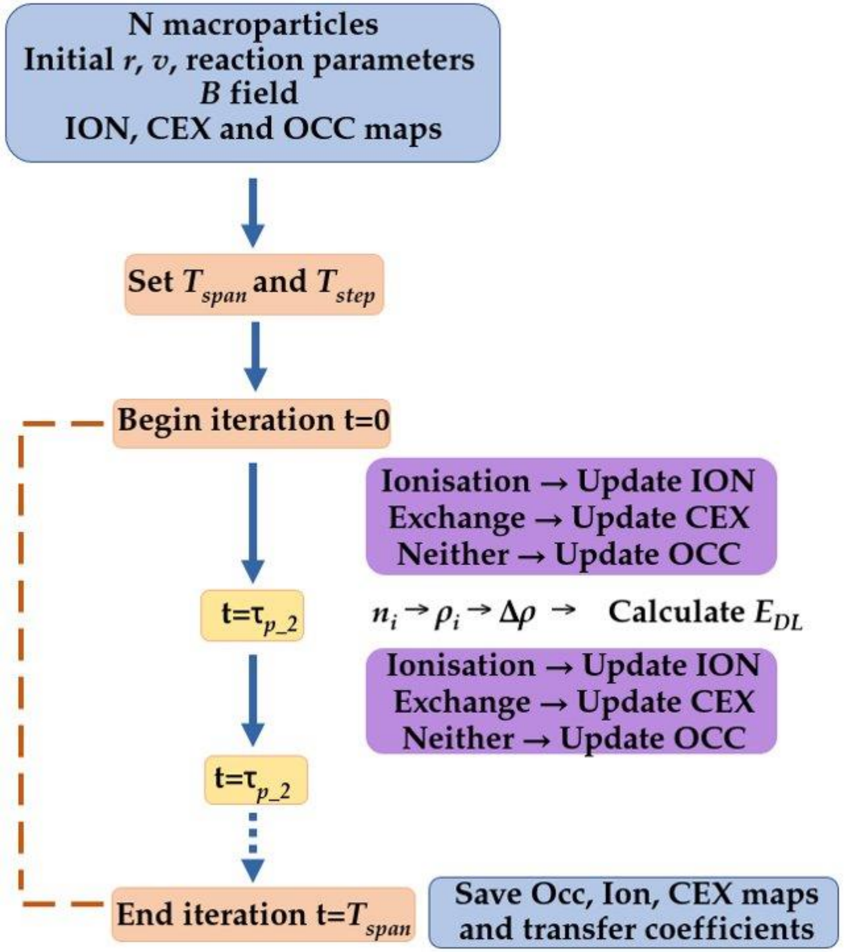

Self-Consistent Electron-Ion Simulations

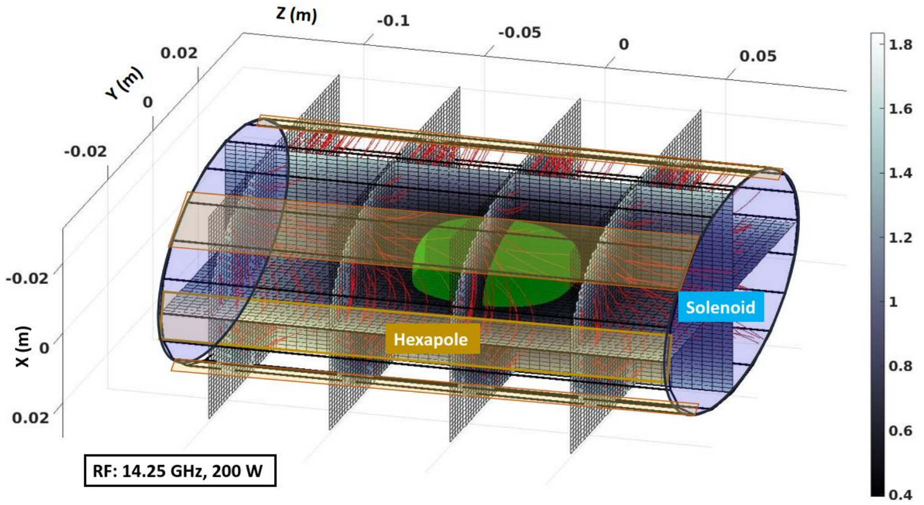

3D view of min-B profile with streamlines of field flow (left) [12] and self-generated double layer electrostatic field (right)

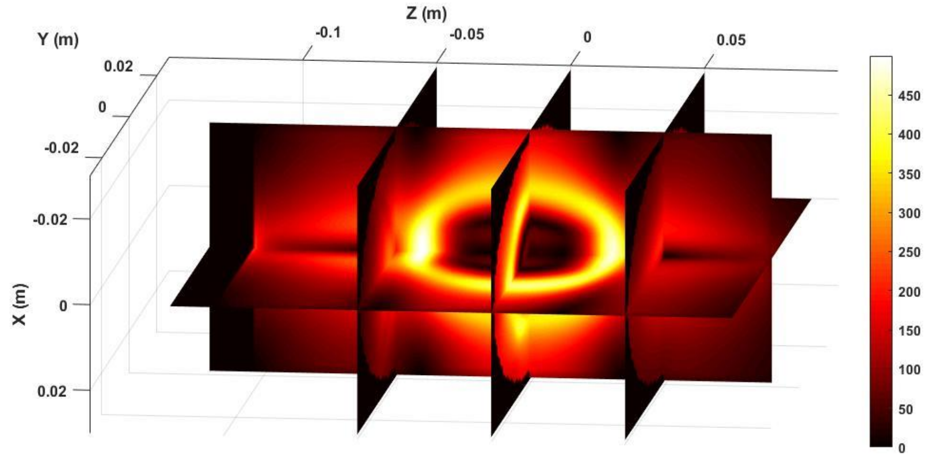

BORIS METHOD

Set of equations for transporting particles under Lorentz force

$$1:\quad x^{n+\frac{1}{2}} = x^n + \frac{\Delta t}{2}\frac{u^n}{\gamma^n}, \qquad u^n = u^n,$$

$$2:\quad x^{n+\frac{1}{2}} = x^{n+\frac{1}{2}}, \qquad u^- = u^n + \varepsilon\Delta t,$$

$$3:\quad x^{n+\frac{1}{2}} = x^{n+\frac{1}{2}}, \qquad u^+ = Ru^-,$$

$$4:\quad x^{n+\frac{1}{2}} = x^{n+\frac{1}{2}}, \qquad u^{n+1} = u^+ + \varepsilon\Delta t,$$

$$5:\quad x^{n+1} = x^{n+\frac{1}{2}} + \frac{\Delta t}{2}\frac{u^{n+1}}{\gamma^{n+1}}, \qquad u^{n+1} = u^{n+1}.$$

LANGEVIN EQUATION

Formalism for including diffusion and friction forces for velocity evolution

$$D_\parallel = \langle \mathbf{v}_\parallel^2 \rangle = \frac{A_D}{|\mathbf{v}^{n+1/2}|} G\left(\frac{|\mathbf{v}^{n+1/2}|}{c_s}\right),$$

$$D_\perp = \langle \mathbf{v}_\perp^2 \rangle = \frac{A_D}{|\mathbf{v}^{n+1/2}|} \left\{ \Phi\left(\frac{|\mathbf{v}^{n+1/2}|}{c_s}\right) - G\left(\frac{|\mathbf{v}^{n+1/2}|}{c_s}\right) \right\}$$

$$\nu_s = \left(1 + \frac{m}{m_s}\right) \frac{A_D}{c_s^3} \frac{G\left(\frac{|\mathbf{v}^{n+1/2}|}{c_s}\right)}{\frac{|\mathbf{v}^{n+1/2}|}{c_s}},$$

where

$$A_D = \frac{(ZZ')^2 e^4 n_s \ln\Lambda}{2\pi\epsilon_0^2 m^2},$$

$$\mathbf{v}_{fric} = \nu_s \mathbf{v}^{n+1/2} T_{step},$$

$$\mathbf{v}_{rand} = P_\parallel N(0, D_\parallel) + P_\perp N(0, D_\perp)$$

$$\mathbf{v}^{n+3/2} = \frac{1}{\gamma}\left(\mathbf{u}^+ + \frac{q}{2m}\mathbf{E}^{n+1} T_{step}\right) + \mathbf{v}_{fric} + \mathbf{v}_{rand}$$

[12] B. Mishra, EPJ Web of Conferences, 2022.

Self-Consistent Electron-Ion Simulations

MONTE CARLO SAMPLING

Formalism for sampling from multiple competing processes

$$\nu_{CEX} = n_0 \sigma_{CEX} v_i$$ **Process 1 (ionisation)**

$$\nu_{ion} = n_e \sigma_{ion} v_e$$ **Process 2 (exchange)**

Effective reaction frequency

$$\nu_{tot} = \nu_{ion} + \nu_{CEX}$$

MC Sampling

$$\text{Ionisation if } 0 <= r < P_{ion}$$

$$\text{CEX if } P_{ion} <= r < P_{ion} + P_{CEX}$$

$$\text{Nothing if } P_{ion} + P_{CEX} <= r < 1$$

$$P_{ion} = \frac{\nu_{ion}}{\nu_{tot}}(1 - e^{-\nu_{tot}\Delta T})$$ **Sampling from process 1 in Δt**

$$P_{CEX} = \frac{\nu_{CEX}}{\nu_{tot}}(1 - e^{-\nu_{tot}\Delta T})$$ **Sampling from process 2 in Δt**

CSD AND DENSITY SCALING

ION NUMBER DENSITY ⟷ **ELECTRON NUMBER DENSITY**

$$\oint_V n_e dV = K_3 \Big[(1 - k_{1\to2} + 2k_{1\to2}k_{2\to1} + k_{1\to2}k_{2\to3}k_{3\to2}) \oint_V n_1 dV +$$
$$2k_{1\to2}(1 - k_{2\to3} - k_{2\to1} + k_{2\to3}k_{3\to2}) \oint_V n_2 dV +$$
$$3k_{1\to2}k_{2\to3}(1 - k_{3\to4} - k_{3\to2}) \oint_V n_3 dV +$$
$$4k_{1\to2}k_{2\to3}k_{3\to4} \oint_V n_{3\to4} dV \Big]$$

$$N_1 = K_3(1 - k_{1\to2} + 2k_{1\to2}k_{2\to1} + k_{1\to2}k_{2\to3}k_{3\to2})n_1$$
$$N_2 = K_3 k_{1\to2}(1 - k_{2\to3} - k_{2\to1} + k_{2\to3}k_{3\to2})n_2$$
$$N_3 = K_3 k_{1\to2}k_{2\to3}(1 - k_{3\to4} - k_{3\to2})n_3$$

$$\rho_\Delta = e[n_e - (N_1 + 2N_2 + 3N_3)]$$

Self-Consistent Electron-Ion Simulations

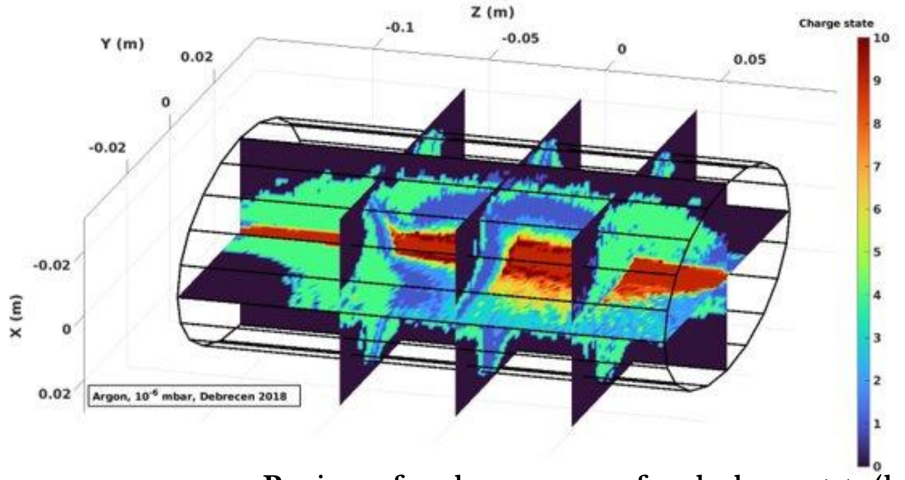

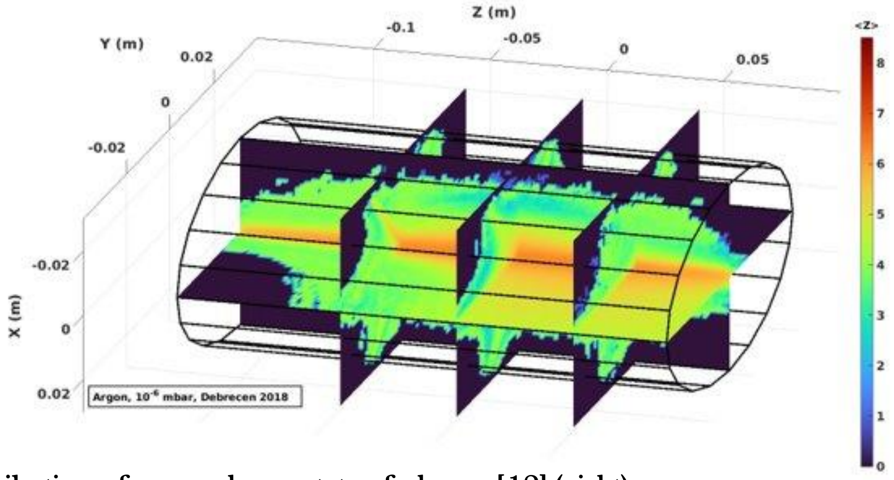

Regions of peak occupancy of each charge state (left) and 3D distribution of mean charge state of plasma [12] (right)

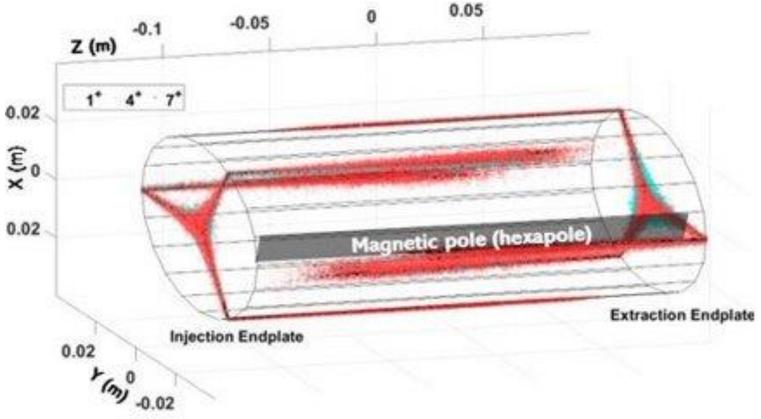

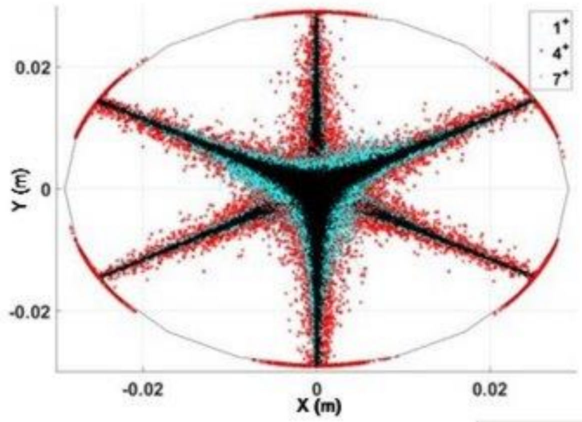

Scatter plot of lost macroparticles corresponding to different charge states [9]

[9] B. Mishra *et al*, Frontiers in Phys., special issue (2022)
[12] B. Mishra, EPJ Web of Conferences, 2022.

Self-Consistent Electron-Ion Simulations

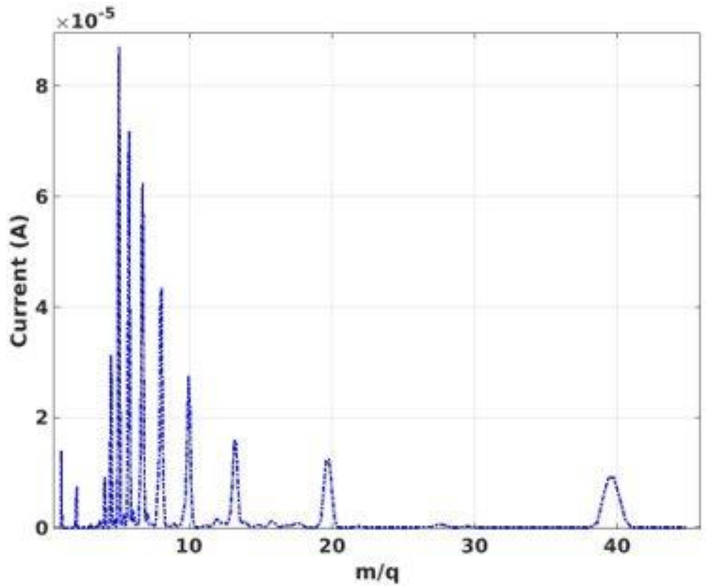

Experimental spectrum of Ar ion current [15]

L = 105 mm

Φ_{ext} = 11 mm

$\langle N_i \rangle$ = Mean density in region of potential dip

$$I_i = \kappa \frac{(2L)S}{2} \frac{\langle N_i \rangle q_i e}{\tau_i}$$

$$\tau_{ES,i} = R \frac{\sqrt{\pi} L}{v_i} \exp\left(\frac{q_i e \langle \phi_{DL} \rangle}{k_B T_i} \right)$$

$$\tau_{d,i} = 7.1 \times 10^{-20} L q_i \ln \Lambda \sqrt{A} \frac{n_e Z_{eff}}{k_B T_i^{3/2} E}$$

$$\frac{1}{\tau_i} = \frac{1}{\tau_{ES,i}} + \frac{1}{\tau_{d,i}}$$

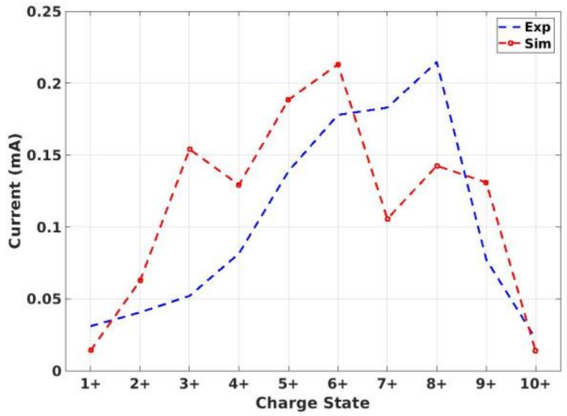

Simulated spectrum of Ar ion current

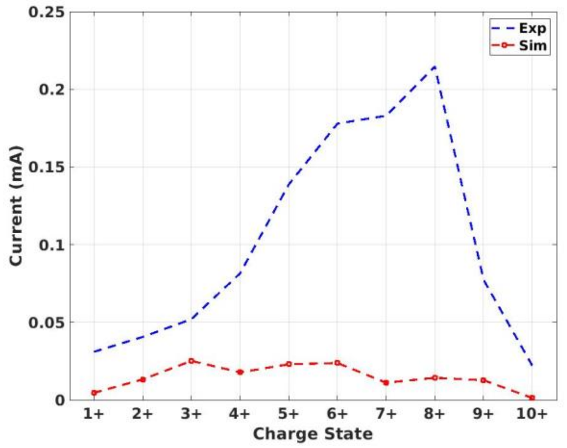

[9] B. Mishra *et al*, Frontiers in Phys., special issue (2022)

[15] S. Biri *et al*, Rev. Sci. Instrum. 83, 02A431 (2012)

Self-Consistent Electron-Ion Simulations

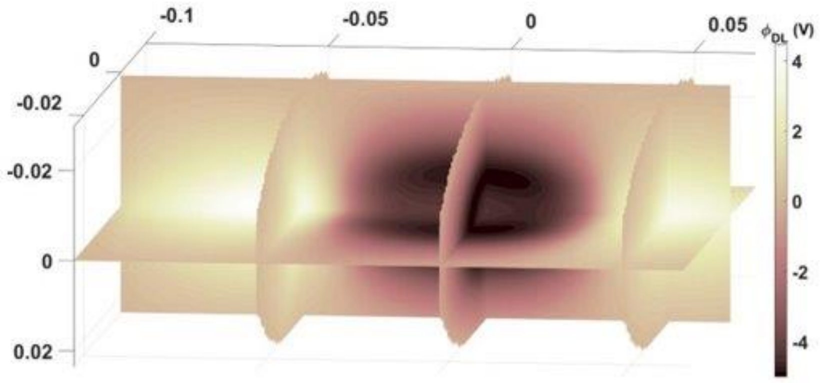

3D distribution of electrostatic potential showing potential dip [9]

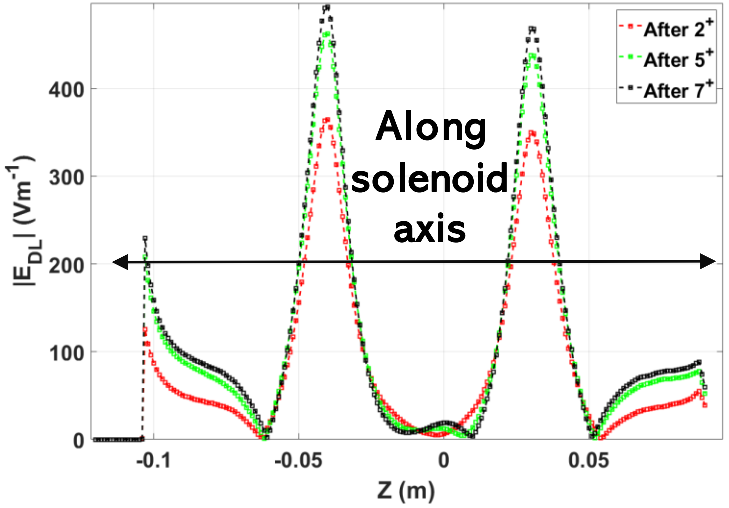

1D profile of double layer field along solenoid axis [9]

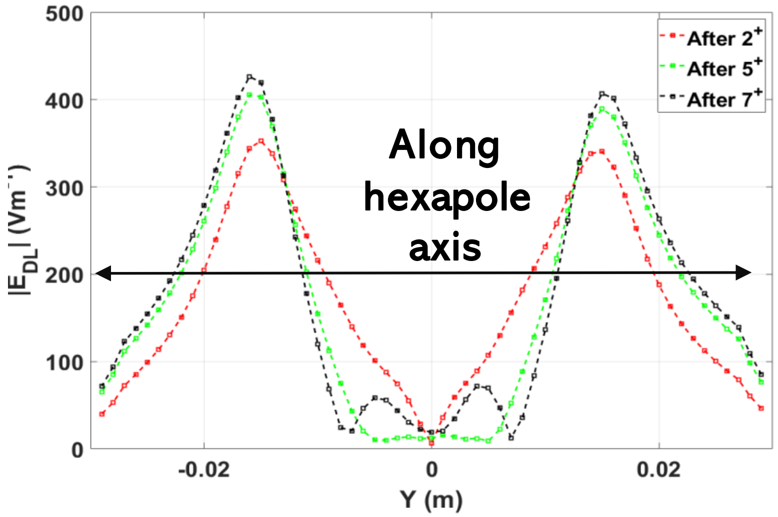

1D profile of double layer field along hexapole axis [9]

ECR plasmas models can advance fundamental research in ECRIS operation

[9] B. Mishra *et al*, Frontiers in Phys., special issue (2022)

Isotope-Plasma Simulations

Same PIC-MC simulation scheme as for plasma ions, but with different balance equation

$$f^*_{IF(m)} = \sum_{ij} p_{ij} \int_1^{W_{max}(ij)} (W^2-1)^{1/2} W (W_{max}(ij)-W)^2 F_0 S_{(m)}(ij) f_d(ij) \mathrm{d}W$$

$$f^*_{IF(m)} = \sum_{ij} p_{ij} \int_{W_{min}(ij)}^{\infty} (W^2-1)^{1/2} W (Q(ij)/m_e c^2)^2 F_0 S_{(m)}(ij) f_c(ij) \mathrm{d}W$$

$$f^*_{IF(m)} = \sum_{ij} p_{ij} \sum_{x(ij)} \sigma_x \frac{\pi}{2} [g_x \, or \, f_x]^2 (Q(ij)/m_e c^2)^2 S_{(m)x(ij)}$$

$$\frac{dn_i^R}{dt} = \left[n_{i-1}^R n_e \gamma_{i-1,i} - n_i^R n_e \gamma_{i,i+1}\right] + \left[n_{i+1}^R \sum_{j=0}^{N-1} n_j E_{i+1,i} + n_{i-1}^R \sum_{j=1}^{N} n_j E_{i-1,i}\right] - \left[n_i^R \sum_{j=0}^{N-1} n_j E_{i,i-1} + n_i^R \sum_{j=1}^{N} n_j E_{i,i+1}\right] - \frac{n_i^R}{\tau_i^R}$$

→ Ionisation and charge exchange for CSD

$$\frac{dn_{ii'}^R}{dt} = \left[\sum_{ij'<ii'} n_{ij'}^R n_e C_{ij'ii'} - n_{ii'}^R \sum_{ij'>ii'} n_e C_{ii'ij'}\right] + \left[\sum_{ij'>ii'} n_{ij'}^R A_{ij'ii'} - n_{ii'}^R \sum_{ij'<ii'} A_{ii'ij'}\right]$$

→ Collisional excitation and spontaneous emission for LPD

~ NLTE model

Soft X-Ray Diagnostics Models

X-ray fluorescence image from SPhC algorithm

$$T = 300\rho_e\rho_i\omega_{K\alpha}\varepsilon_g\varepsilon_q\int_{3.205}^{\infty}\sigma_{K,ion}(E)v(E)f(E)\mathrm{d}E$$

+

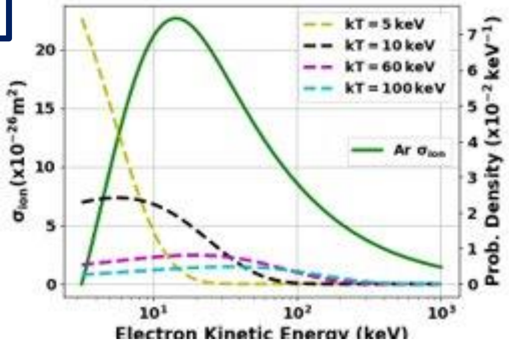

+

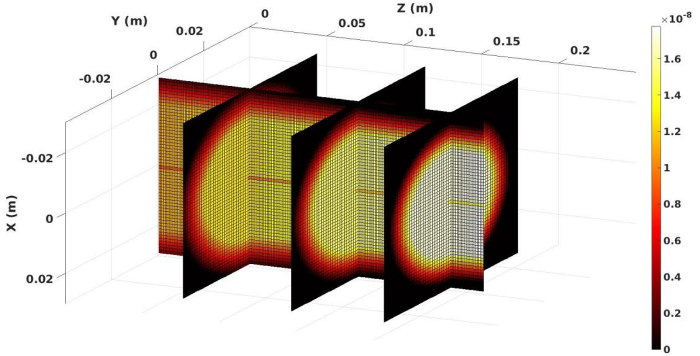

=

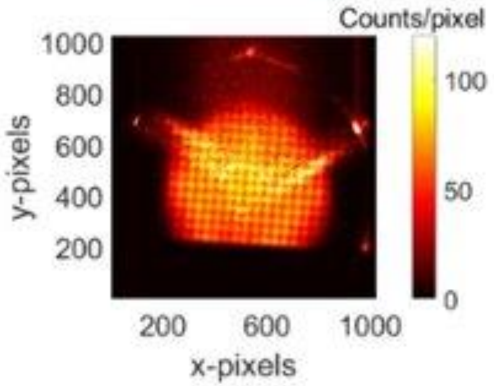

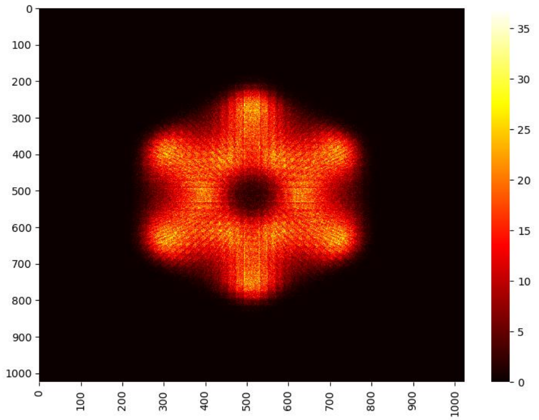

[20] B. Mishra *et al*, Phys. Plasmas, (2021)
[21] B. Mishra *et al*, Condens. Matter, (2021)
[22] S. Biri *et al*, JINST 16, P03003 (2021)

Soft X-Ray Diagnostics Models

X-ray spectrum from SPhC algorithm

$$J(h\nu) = h\nu \frac{N^p(h\nu)}{t} \frac{4\pi}{\Delta E V_P \Omega_g}$$

+

$$J_{theo,brem}(h\nu) = \rho_e \rho_i (Z\hbar)^2 \left(\frac{4\alpha}{\sqrt{6m_e}}\right)^3 \left(\frac{\pi}{k_B T_e}\right)^{1/2} e^{h\nu/k_B T_e}$$

$$J_{theo,line,plasma}(h\nu) = [J_{theo,2.96} D_{PV}(h\nu - 2.96, f_{2.96}) + J_{theo,3.19} D_{PV}(h\nu - 3.19, f_{3.19})]\Delta E$$

+

$$J_{theo,h\nu} = \frac{h\nu}{V_P \Delta E} \rho_{e,loss} N_t \int_I^\infty \sigma_{K,ion}(E) v_e(E) f(E) \mathrm{d}E$$

=

$\rho_e \rho_i$ ~ 1.32x10^{32} m^{-6}, expected ρe ~ 10^{16} m^{-3}
T_e ~ 21.15 keV
$\rho_{e,loss}$ ~ 10^{12} m^{-3}, estimated j_{av} ~ 2-3 mA/cm²
Matches ion current density to order of magnitude

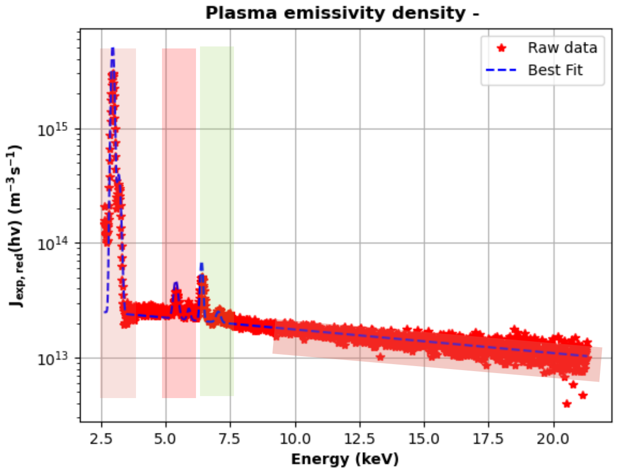

Conclusions and Future Perspectives

ECR plasmas can be reliable systems for emulating stellar environments and reactions thereof

Experimental activities can be complemented by ECR plasma models for optimised analysis

Self-consistent steady state routines developed to describe electrons, ions and radio-isotopes in plasma

In-plasma decay rate formalism already developed

Plasma models (soft X-ray) can also be used to extract electron and ion parameters from spectra

Models useful not only for application like PANDORA but also for fundamental ECRIS research

David Mascali
Domenico Santonocito
Angelo Pidatella
Eugenia Naselli
Giuseppe Torrisi
Giorgio Mauro

Alessio Galatà

Alberto Mengoni

Sara Palmerini
Maurizio Busso

Sandor Biri
Richard Rácz

THANK YOU FOR YOUR ATTENTION!

...the PANDORA collaboration, and everyone here whose work I have used in some way!

Additional Content 1 – Soft X-Ray Spectroscopy

$$T = 300\rho_e\rho_i\omega_{K\alpha}\varepsilon_g\varepsilon_q\int_{3.205}^{\infty}\sigma_{K,ion}(E)v(E)f(E)\mathrm{d}E$$

Evaluating 3D space-resolved electron energy distribution function (EEDF) and analysing behaviour of K-shell ionisation cross-section [6]

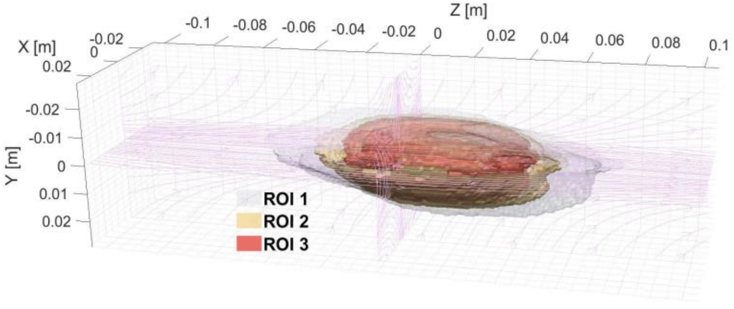

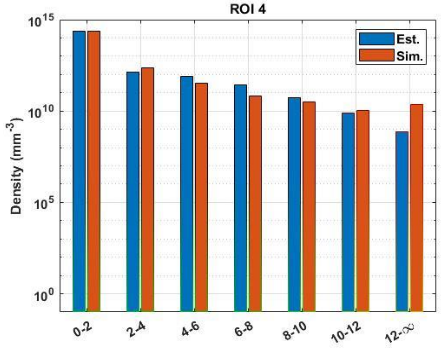

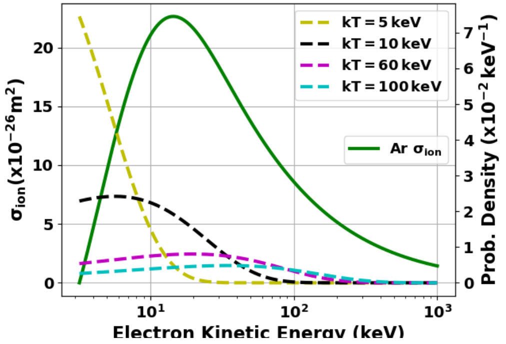

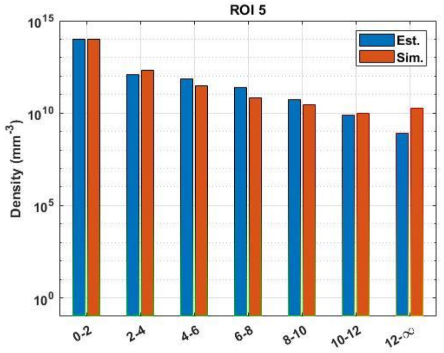

Evaluating 3D space-resolved geometrical efficiency and quantum efficiency of simulation domain [7]

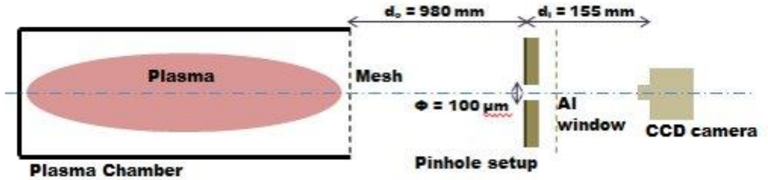

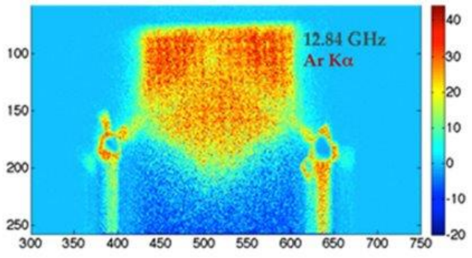

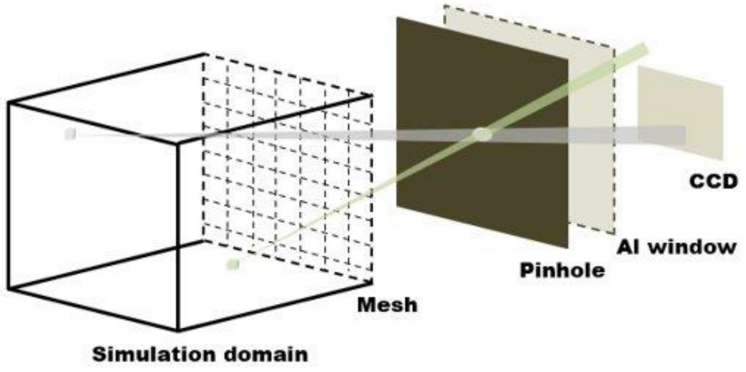

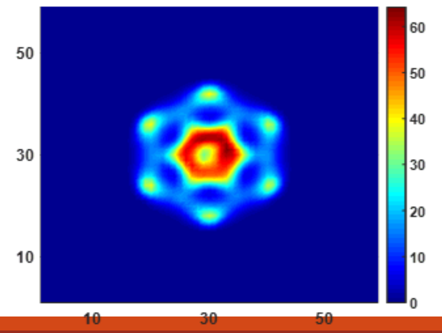

Additional Content 1 – Soft X-Ray Spectroscopy

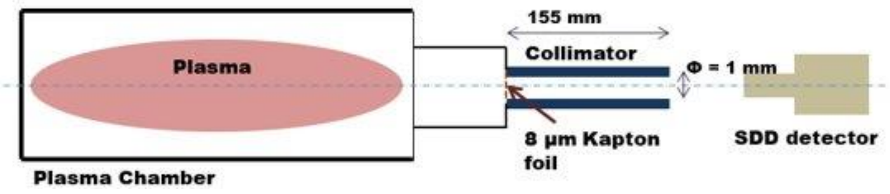

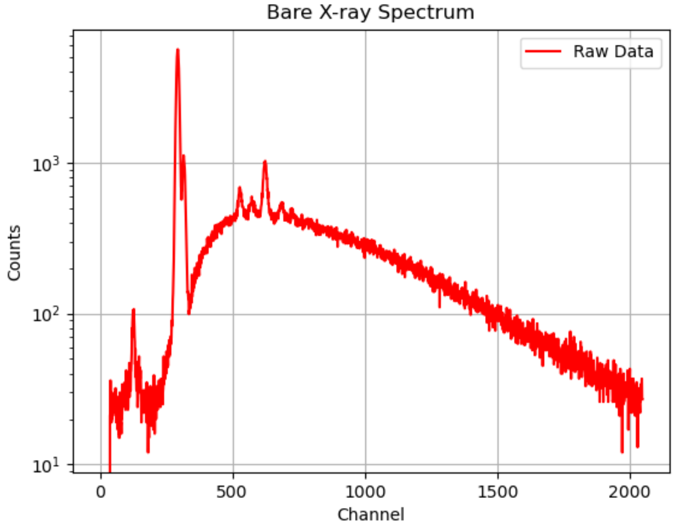

- **Calibration with Fe lines**
- **QE renormalisation**
- **Dead time correction**
- **Conversion to emissivity density**

$$J(h\nu) = h\nu \frac{N^p(h\nu)}{t} \frac{4\pi}{\Delta E V_P \Omega_g}$$

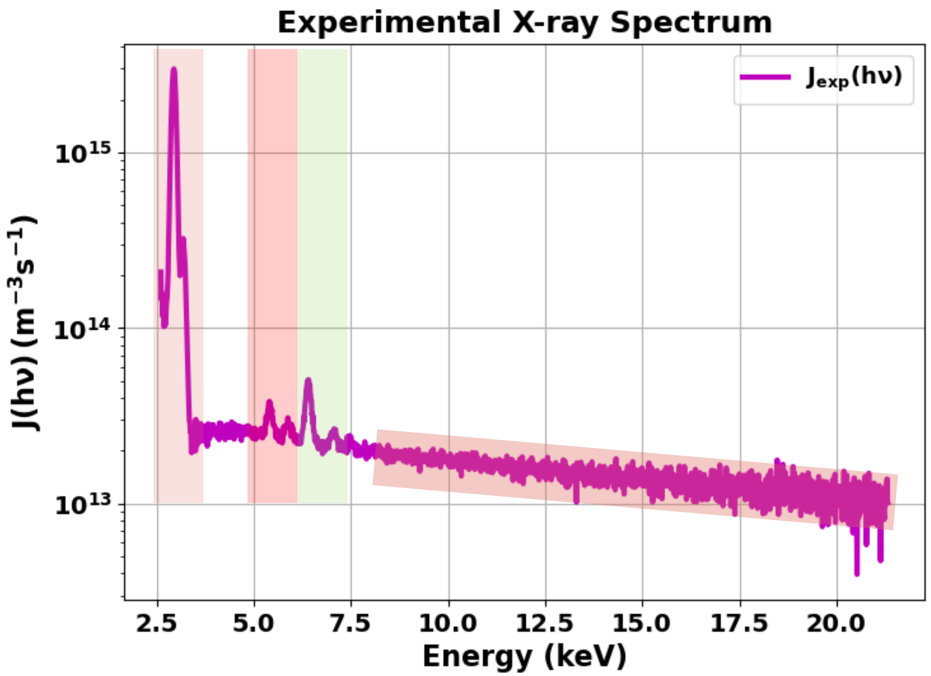

Bremsstrahlung Emissivity Density

$$J_{theo,brem}(h\nu) = \rho_e \rho_i \int_{h\nu}^{\infty} \frac{d\sigma_K(h\nu)}{dh\nu} v_e(E) f(E) dE$$

⇩

Kramer's formula for differential cross section

$$\frac{d\sigma_K(h\nu)}{dh\nu} = \frac{16\pi}{3\sqrt{3}} \alpha^3 \left(\frac{\hbar}{m_e c}\right)^2 \left(\frac{c}{v_e}\right)^2 \frac{Z^2}{h\nu}$$

⇩

Single-component Maxwell EEDF

$$f_M(E; k_B T_e) = \frac{2}{\sqrt{\pi}} \frac{\sqrt{E}}{(\sqrt{k_B T_e})^3} e^{-E/k_B T_e}$$

⇩

$$J_{theo,brem}(h\nu) = \rho_e \rho_i (Z\hbar)^2 \left(\frac{4\alpha}{\sqrt{6 m_e}}\right)^3 \left(\frac{\pi}{k_B T_e}\right)^{1/2} e^{h\nu/k_B T_e}$$

Line Emissivity Density (Ar ions)

$$J_{theo,2.96} = \frac{h\nu_{2.96}}{\Delta E} \rho_e \rho_i \omega_{2.96} \int_{3.205}^{\infty} \sigma_{K,ion}(E) v_e(E) f(E) dE$$

$$J_{theo,3.19} = \frac{h\nu_{3.19}}{\Delta E} \rho_e \rho_i \omega_{3.19} \int_{3.205}^{\infty} \sigma_{K,ion}(E) v_e(E) f(E) dE$$

⇩

Lotz formula for K-shell ionisation cross-section

$$\sigma_{K,ion} = a_K q_K \frac{\ln \varepsilon / I}{\varepsilon I} \{1 - b_K \exp[-c_K(\varepsilon/I - 1)]\}$$

⇩

Pseudo-Voigt profile for line broadening

$$D_{PV}(x - x_0, f) = \eta L(x - x_0, \tau_L) + (1 - \eta) G(x - x_0, \sigma_G)$$

⇩

$$J_{theo,line,plasma}(h\nu) = [J_{theo,2.96} D_{PV}(h\nu - 2.96, f_{2.96}) + J_{theo,3.19} D_{PV}(h\nu - 3.19, f_{3.19})]\Delta E$$

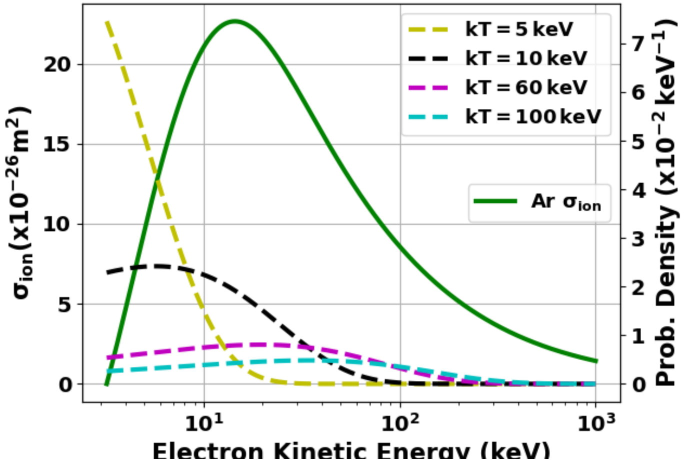

Lotz cross-section for Ar superposed on Maxwell EEDFs at different temperatures [6]

[6] B. Mishra *et al*, Phys. Plasmas, (2021)

Electron Diagnostics – X-Ray Spectroscopy - Volumetric

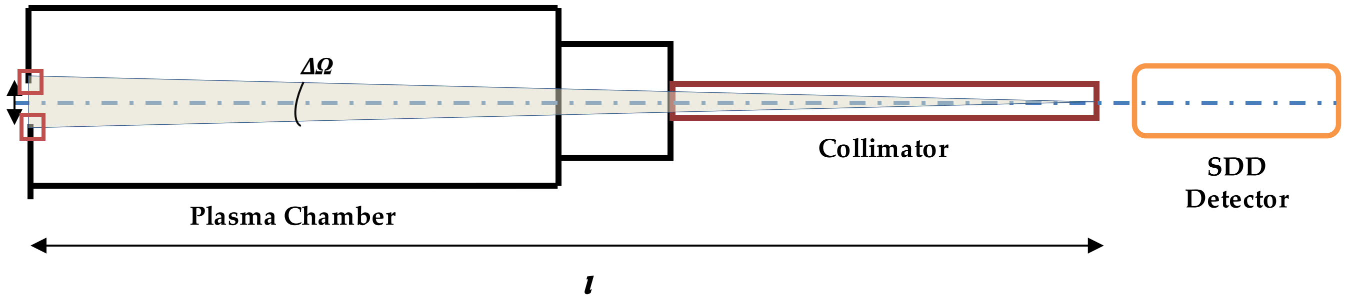

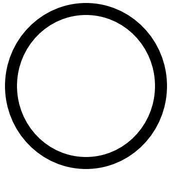

Active emission area = $4\pi\varepsilon_{gl}^{2} - \pi d^2/4$

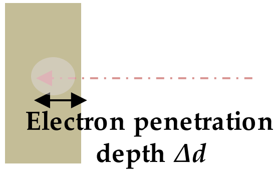

$$J_{theo,h\nu} = \frac{h\nu}{V_P \Delta E}\rho_{e,loss} N_t \int_I^\infty \sigma_{K,ion}(E) v_e(E) f(E) \mathrm{d}E$$

Deutsch-Mark formalism for K-shell ionisation cross-section

$$\sigma_{1s,ion} = g_{1s}\pi (r_{1s})^2 \xi_{1s} f(U) F(U)$$

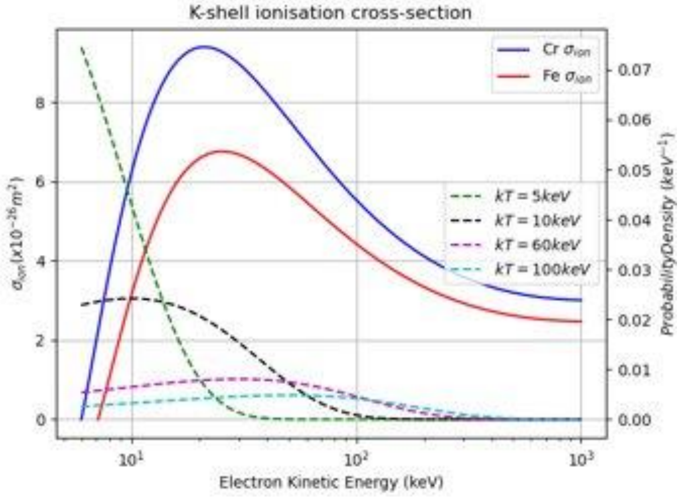

DM cross-section for Cr/Fe superposed on Maxwell EEDFs at different temperatures [6]

Estimation of number of target atoms N_t

$$N_t(E) = n_t\left(4\pi\varepsilon_g l^2 - \pi\frac{d^2}{4}\right)\Delta d(E)$$

Parametrisation of penetration depth as a function of energy

$$J_{theo,h\nu} = \frac{h\nu}{V_P \Delta E}\rho_{e,loss} n_t \left(4\pi\varepsilon_g l^2 - \pi\frac{d^2}{4}\right)\int_I^\infty v_e(E) f(E) \int_E^I \frac{1}{S(E)}\sigma_{K,ion}(E')\mathrm{d}E'\mathrm{d}E$$

$$J_{theo,line,loss}(h\nu) = \sum J_{theo,h\nu_0} D_{PV}(h\nu - h\nu_0, f_{h\nu_0})\Delta E$$

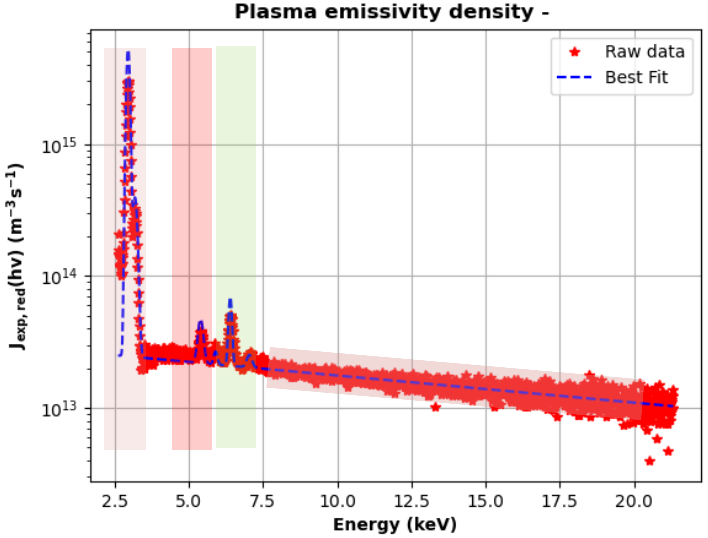

$\rho_e\rho_i$ ~ 1.32x10^{32} m^{-6}, expected ρe ~ 10^{16} m^{-3}
T_e ~ 21.15 keV
$\rho_{e,loss}$ ~ 10^{12} m^{-3}, estimated j_{av} ~ 2-3 mA/cm^2
Matches ion current density to order of magnitude

[6] B. Mishra *et al*, Phys. Plasmas, (2021)

Objective: Launch electron simulations for higher energy ranges and compare model-generated maps with experiment again

SECOND ATTEMPT
DATA: Debrecen 2018

Electron data stored in 7 new intervals:
[1,15], [15,29], [29,43], [43-57], [57,71], [71,85] and [85,∞] keV

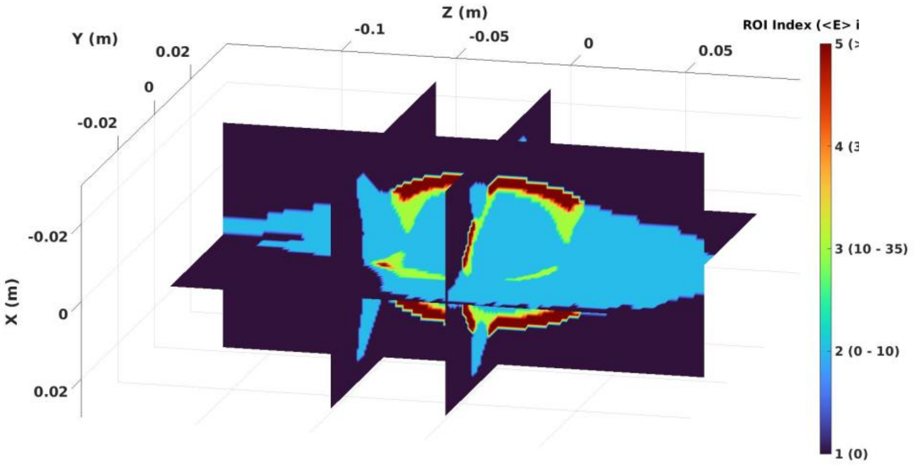

Mean electron energy-based ROIs generated for Debrecen 2018 plasma

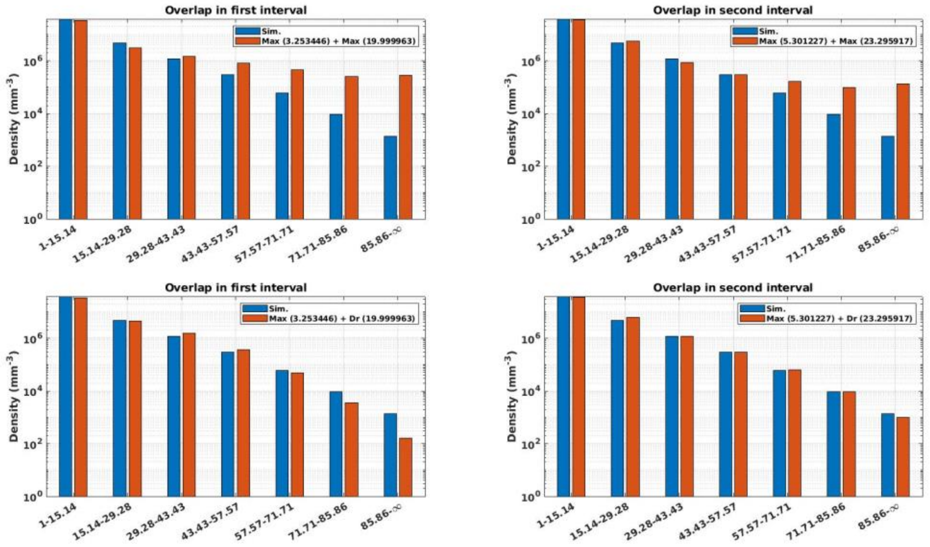

Qualitative EEDF fit of ROI 2 – best function Maxwellian+Druyvesteyn

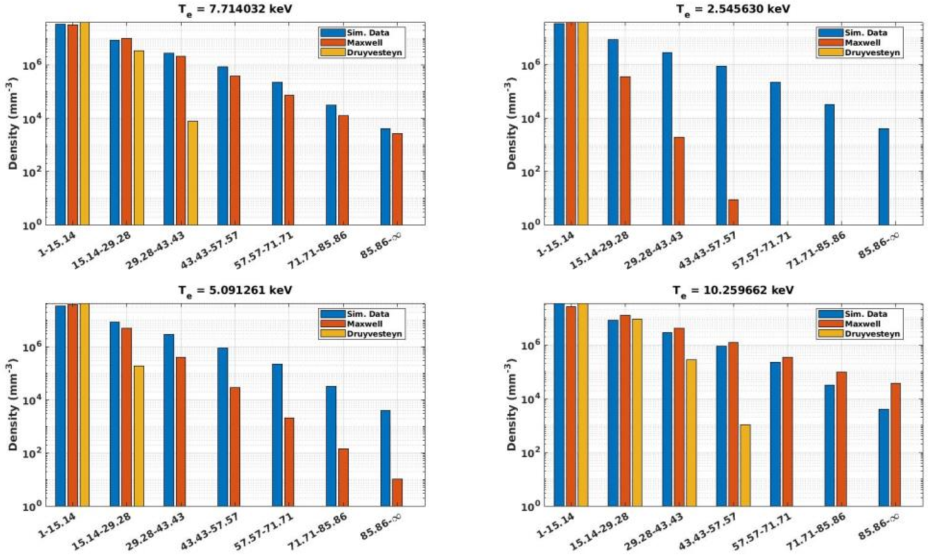

Qualitative EEDF fit of ROI 3 – best function Maxwellian

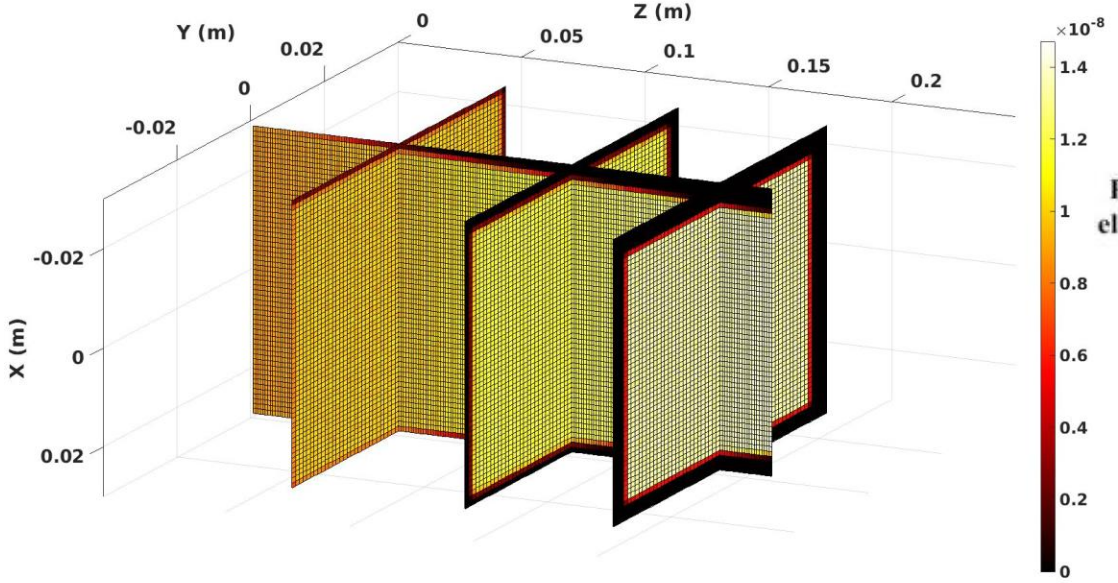

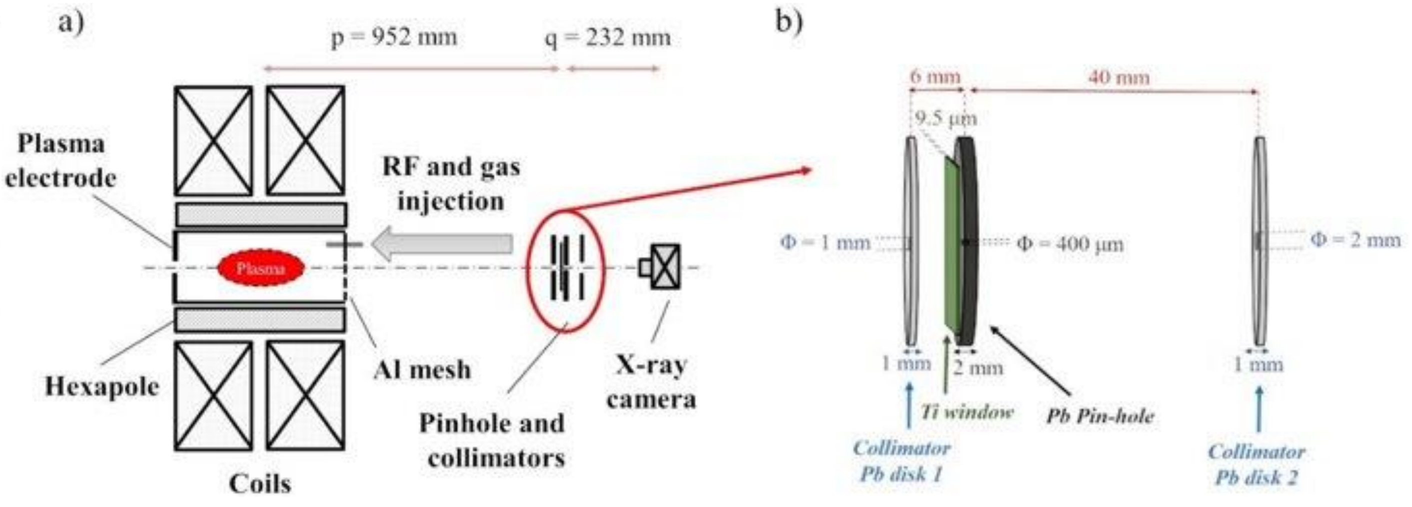

Schematic of multi-collimator CCD-pinhole setup used in Debrecen 2018 [9]

Local geometrical efficiency calculated using the ray-tracing Monte Carlo method without multi-collimator (top) and with multi-collimator (bottom) - enhanced screening and resolution

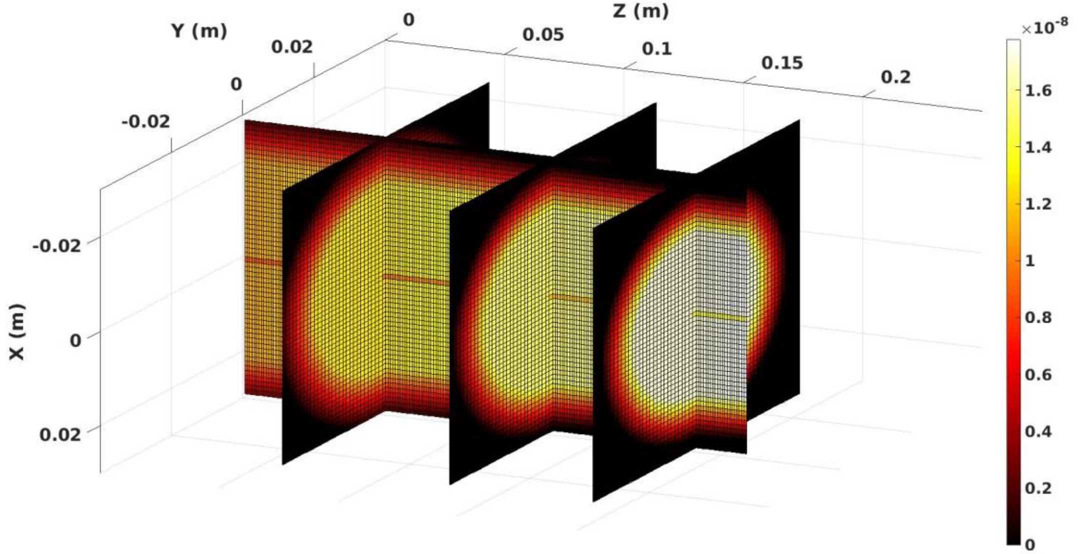

- **3D space-resolved charge density and EEDF**
- **K-shell ionisation cross-section**
- **Local geometrical efficiency**

[9] S. Biri *et al*, JINST 16, P03003 (2021)

Electron Diagnostics – X-Ray Spectroscopy - Fluorescence

Space-resolved energy density + **K-Shell ionisation cross-section** + **Local geometrical efficiency**

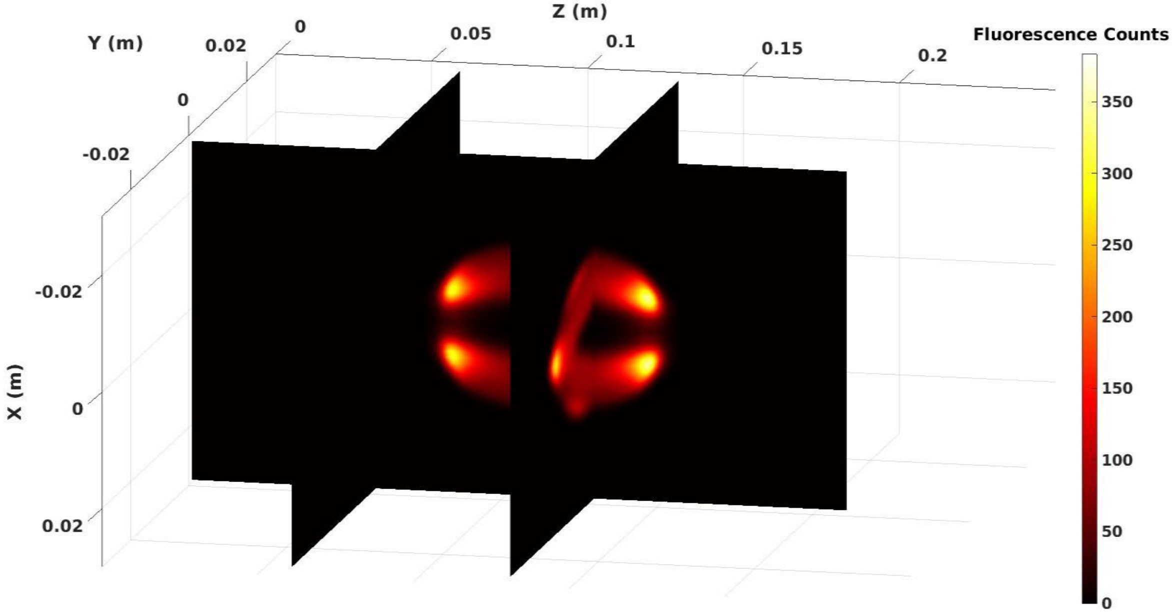

Simulated emission map from Debrecen 2018 configuration

Generating image of X-ray map on CCD – 1024x1024 pixels

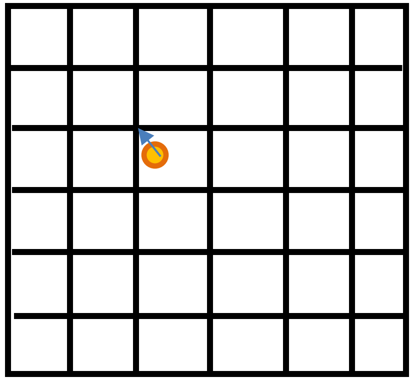

Grid of 1024 x 1024 points
Map photon to nearest grid point (0th order approximation)

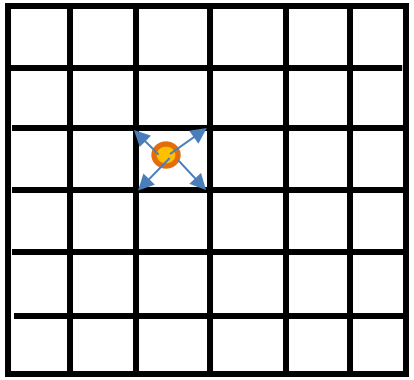

Grid of 1024 x 1024 points
Map photon to nearest neighbour grid points (1st order approximation)

Electron Diagnostics – X-Ray Spectroscopy - Fluorescence

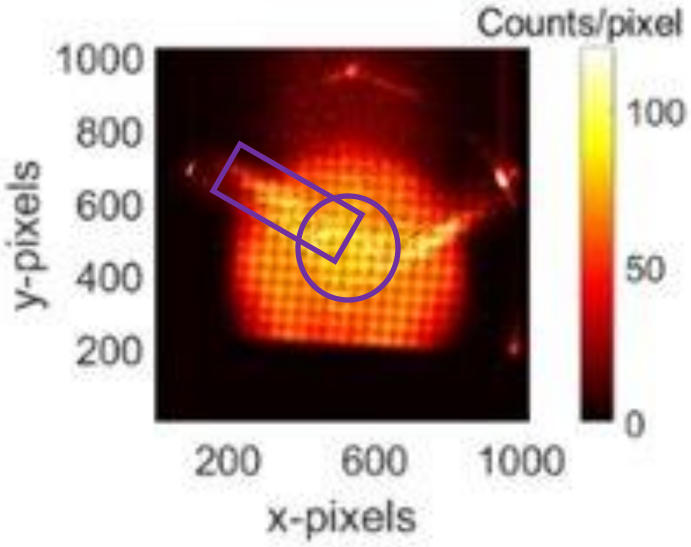

Experimental fluorescence map [9]

1st order projection

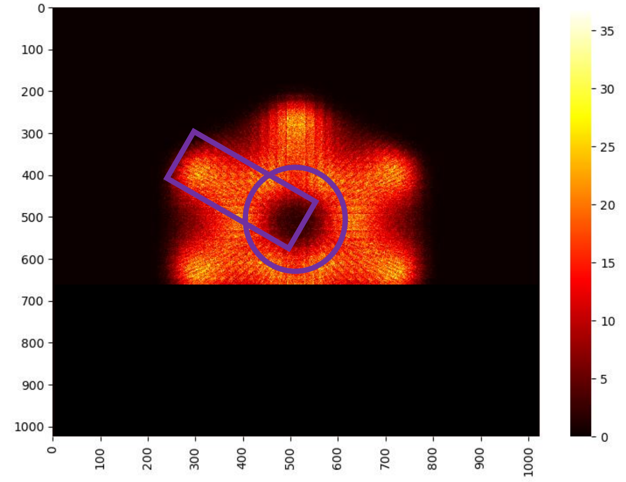

0th order projection

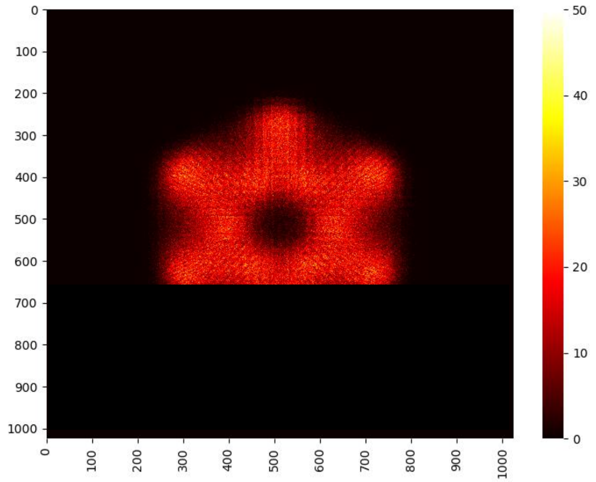

Conclusions:

New method for resolving plasma non-homogeneity established, allowing quantitative study of EEDF on a ROI-by-ROI basis

Match between experiment and model much better for Debrecen 2018 as compared to Debrecen 2014 – electron density on correct order of magnitude, general features reproduced

Some aspects not reproduced – notably the hole in the centre – can be attributed to incompleteness of electron simulations

Only 3 magnetic branches visible in experiment – may be attributed to ion density distribution, incomplete implementation of clusterisation

Upgrades underway:

- Update PIC code to generate realistic electron and ion maps
- New correct emission rates using space-resolved EEDFs
- Implement features like mesh and clustering in CCD projection
- Formalism to obtain fluorescence + bremsstrahlung from specific regions at CCD for more complete benchmarking

[9] S. Biri *et al*, JINST 16, P03003 (2021)

Additional Content 2 – Level Grouping

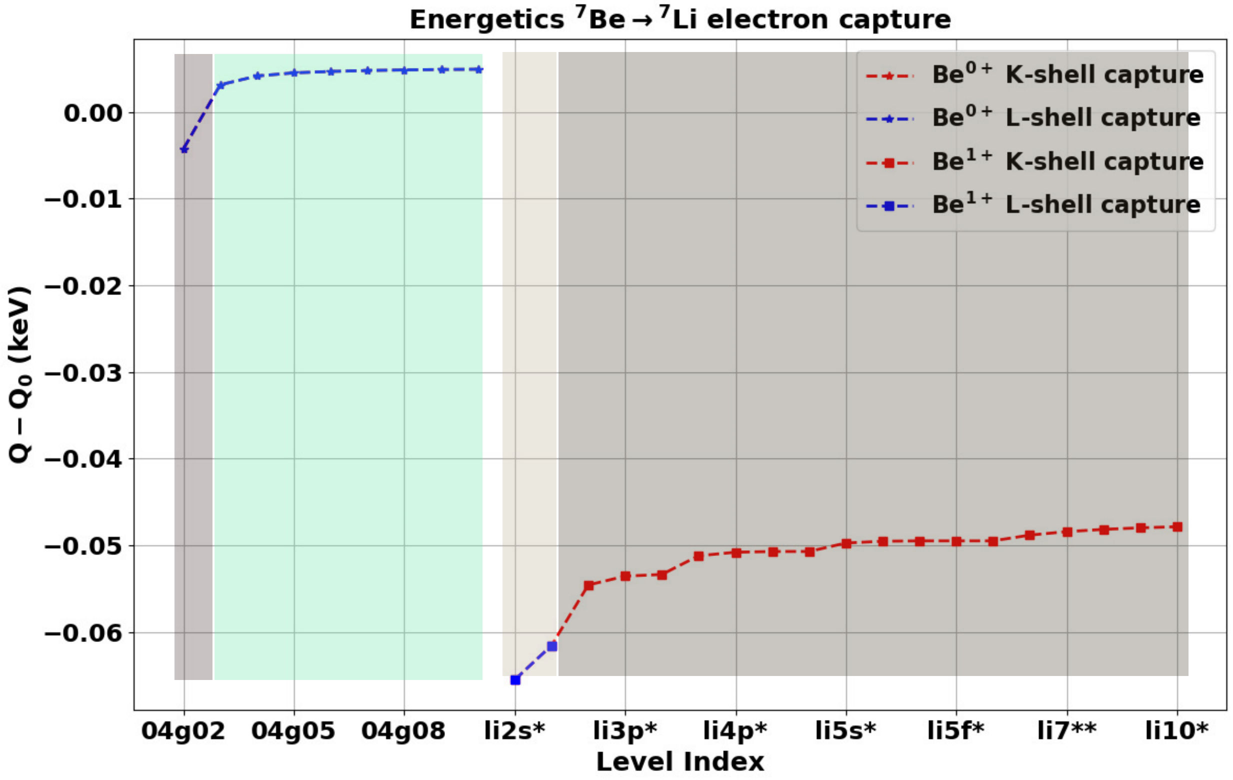

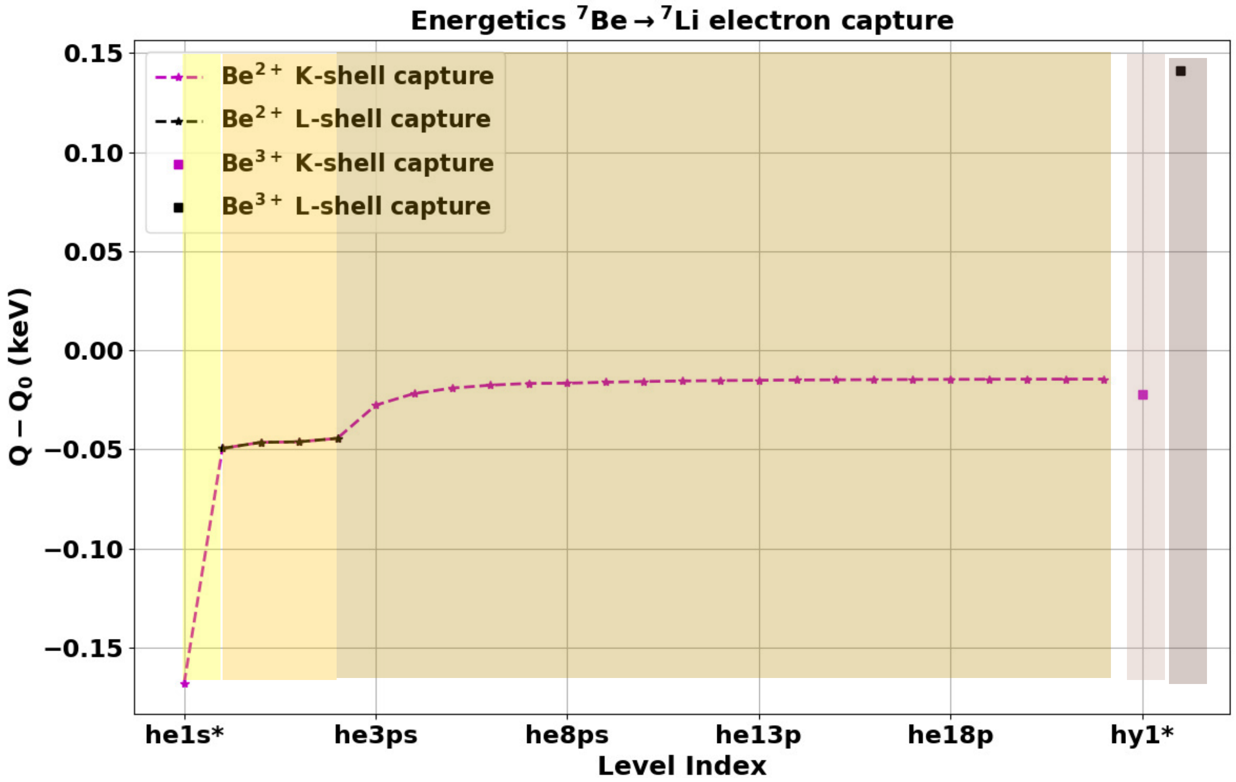

Additional Content 2 – Level Grouping

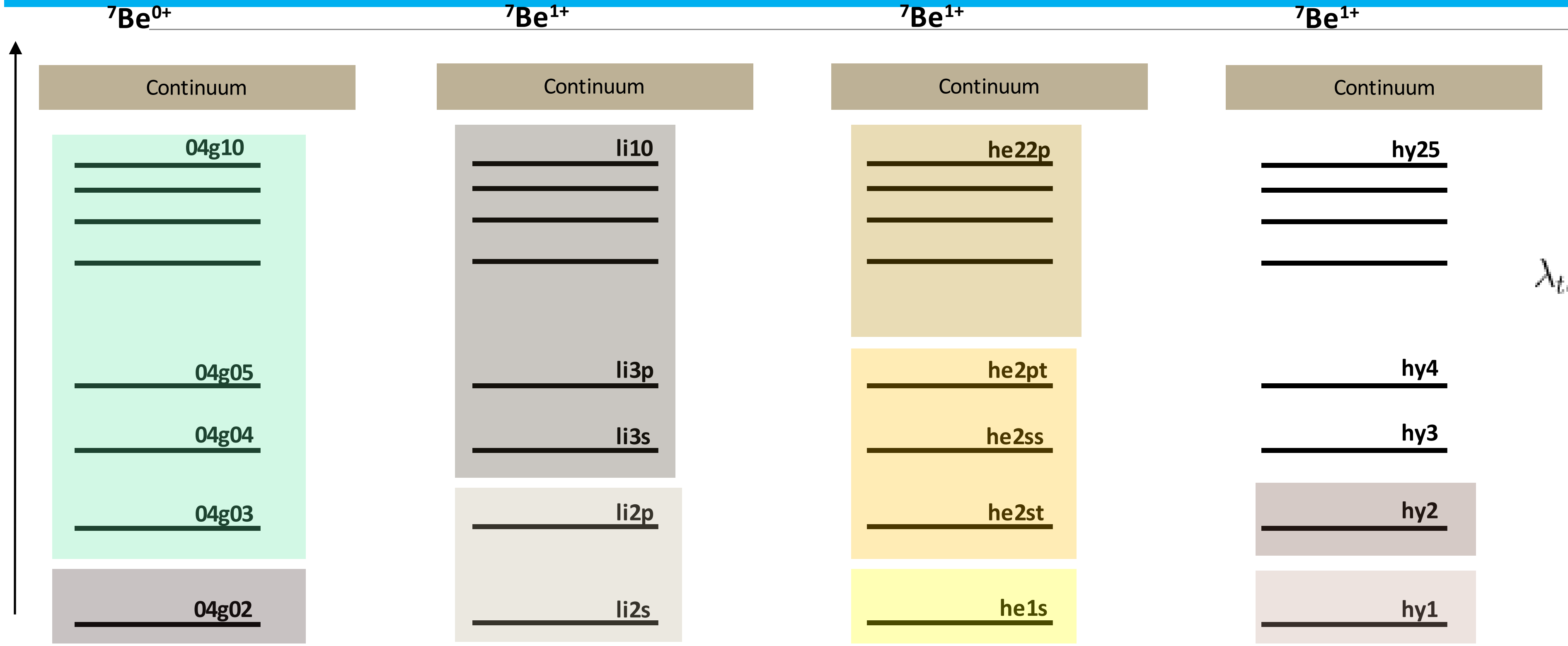

$$\lambda_{tot} = \left[\frac{\ln 2}{f_{IF(m)} t_{1/2}}\right] \sum f^{*}_{IF(m)}$$

Nuclear Matrix Element (NME) from decay tables

- **Use grouped levels as super-groups for calculating reaction rates**
- **Variations within each super-group do not affect decay rates significantly – only ratio of population in each does**
- **Reaction rate matrix to be solved till steady-state – final population represent plasma equilibrium**

Only parent system can be studied